Petroleum Science 19 (2022) 2941–2958

Contents lists available at ScienceDirect

Petroleum Science

journal homepage: www.keaipublishing.com/en/journals/petroleum-science

Original Paper

Plugging performance and mechanism of an oil-absorbing gel for lost circulation control while drilling in fractured formations

Ying-Rui Bai [a], Li-Yao Dai [a], Jin-Sheng Sun [a, b, *], Guan-Cheng Jiang [c], Kai-He Lv [a], Rong-Chao Cheng [b], Xiao-Sen Shang [a]

[a] School of Petroleum Engineering, China University of Petroleum (East China), Qingdao, 266580, Shandong, China
[b] CNPC Engineering Technology R&D Company Limited, Beijing, 102206, China
[c] College of Petroleum Engineering, China University of Petroleum (Beijing), Beijing, 102249, China

ARTICLE INFO

Article history:
Received 27 December 2021
Received in revised form
5 August 2022
Accepted 8 August 2022
Available online 15 August 2022

Edited by Yan-Hua Sun

Keywords:
Lost circulation
Oil-absorbing gel
Oil absorption capacity
Plugging mechanism
Fractured formation

ABSTRACT

Lost circulation of drilling fluid is one of the most common engineering problems in the drilling process of fractured formations. In this study, an oil-absorbing polymer gel synthesized using compound monomers with rigid and flexible chains was applied to control the oil-based drilling fluid loss while drilling. The microstructure, oil-absorbing performance, and plugging performance the gel was investigated. A large number of dense pores on the surface of the gel were observed, which allowed the oil molecules to enter the internal space of the gel. The initial oil absorption capacity of the gel was fast, and it increased with the increase in the temperature and decrease in the particle size, reaching 20.93 g/g at 140 °C. At a high temperature of 140 °C, the bearing pressure capacity of the gel formula containing particles of different particle sizes reached 7.6 MPa for a fracture of a width of 3 mm, showing that the oil-absorbing gel have excellent plugging performance at high temperature. Plugging mechanism of the gel was investigated through visualized fracture plugging experiments. Results show that the dynamic migration, particle-swelling, particle-bridging, particle-aggregation, deformation-filling, and compaction-plugging contribute to the whole lost circulation control process, reflecting that the plugging performance can be effectively enhanced by improving the aggregation and filling degrees of the gel with different particle sizes.

1. Introduction

During various downhole operations such as drilling and cementing, the working fluid in the wellbore enters the formation under differential pressure. This situation resulting in the loss of the working fluid is called lost circulation (Cui et al., 2021; Ezeakacha et al., 2018). Lost circulation is one of the most common downhole complications in the oil drilling process (Wang et al., 2020a,b). Based on the lost circulation channel type, lost circulation can be classified as seepage lost circulation and fracture lost circulation. The occurrence rate of lost circulation in the world is about 20%–25% of the total drilling wells, and it causes a significant economic loss to the global oil industry each year, as high as 40 × 10^8 US dollars per year (Calçada et al., 2015; Feng et al., 2018). The downtime caused by lost circulation accounted for more than 70% of the total downtime caused by complicated drilling accidents from 2017 to 2018, and the average annual economic loss caused by lost circulation amounted to more than 40 × 10^8 CNY (Sun et al., 2021). Severe lost circulation accidents often happen in fractured formations, and the success rate of one-time job in fractured formations is low. The success rate of one-time job is lower than 40% in the Tarim Kuqa Piedmont region, and smaller than 20% in the Permian Formation Khuff fractured formation of Ghawar oilfield, Saudi Arabia (Lavrov, 2016; Sun et al., 2021). Therefore, severe lost circulation occurring in fractured formations is difficultly controlled and it has become an urgently-needed problem. Therefore, the scientific and efficient management of lost circulation in fractured formations is crucial for improving drilling efficiency and reducing drilling costs.

Owing to the advantages of inhibition, high lubricity, and

* Corresponding author. School of Petroleum Engineering, China University of Petroleum (East China), Qingdao, 266580, Shandong, China.
E-mail address: sunjsdri@cnpc.com.cn (J.-S. Sun).

https://doi.org/10.1016/j.petsci.2022.08.004

thermal stability, oil-based or synthetic-based drilling fluids can better meet the drilling requirements in water-sensitive formations compared to water-based drilling fluids (Li et al., 2016; Jiang et al., 2021, 2022). When the oil-based drilling fluid wets the fracture wall, because of the high lubricity of oil compared with water, the lost circulation materials are not easy to accumulate and stay in the fracture, increasing the difficulty of lost circulation control. To solve the lost circulation problem of drilling fluids, extensive studies have been conducted over the years, and many types of lost circulation materials have been developed, including bridging material, high water-loss material, water/oil-absorbing swellable material, gel material, and curable material, etc. (Sun et al., 2021; Pang et al., 2022). In contrast, gel and curable materials are suitable for plugging fractured formation with large loss, bridging, high water-loss, and water/oil-absorbing swellable materials are applied to plugging fractured formation with moderate or small losses. Moreover, the water/oil-absorbing swellable material can be used to plug fractures while drilling, other types of materials are mainly used when drilling is stopped (Lavrov, 2016; Chen et al., 2021).

Compared with lost circulation materials for water-based drilling fluid, there are fewer kinds of lost circulation materials suitable for oil-based drilling fluid at present (Bai et al., 2021a). Oil-based crosslinked gel, oil-absorbing swellable material, oleophilic resin, surface-hydrophobic modified bridging material are mainly used for oil-based drilling fluid (Tariq et al., 2022). In contrast, oil-based crosslinked gel and surface-hydrophobic modified bridging material (walnut shells, asphalt particles, and oleophilic graphite) are suitable for plugging fractured formation with large and moderate losses, respectively, oil-absorbing swellable material and oleophilic resin are applicable to plugging formations with small loss while drilling. Researchers have conducted large numbers of experimental studies about lost circulation materials for oil-based drilling fluids. Chen et al. (2021) designed and synthesized an amine crosslinked polymer lost circulation material (ACP) by crosslinking poly(maleic anhydride-alt-1-octadecene) with amine. The hyper-crosslinked copolymer structure enabled the ACP polymer to withstand a high temperature of 232 °C. Moreover, a mass concentration of 3% was sufficient to effectively reduce the lost circulation of a drilling fluid. Li et al. (2020) synthesized a styrene–butadiene resin/nanosilica composite emulsion as a lost circulation material, which can be dispersed in water and vegetable oil to exert a lost circulation control effect. Qiu et al. (2022) synthesized an oil-based gel lost circulation material with high structural strength and thermal stability using butyl methacrylate and butyl acrylate as raw materials. The bearing pressure capacity of this material for a fracture of a width of 6 mm was 3.01 MPa with a bearing pressure gradient of 0.602 MPa/cm. Currently, the combination of lost circulation control with drilling and bearing pressure plugging for the lost circulation problem of oil-based drilling fluids has been applied, and certain effects have been achieved.

Stress-cage theory and tight plugging mechanism are two main mechanisms related to the lost circulation control in fractures (Sun et al., 2021). Stress-cage theory was proposed by Aston et al. (2004) for borehole reinforcement, which mainly suitable for plugging fracture formations with small loss. This method requires the lost circulation material have a certain amount of compressive strength to form a plugging layer near the fracture entrance, block the transfer of drilling fluid pressure and fluid medium, increase the circumferential stress, form a stress cage, and then enhance the bearing pressure capacity of the formation (van Oort et al., 2018). The main connotation of tight plugging mechanism is that the lost circulation materials form a stable and compact structure in fractures. Kang et al. (2014) reported that the lost circulation material, particle groups in the force chain network, and the plugging layer in the fracture lost circulation channel constitutes the multiscale structure of the fracture plugging layer. Xu et al. (2021b) reported that the microscopic force chain network is the intrinsic mechanism of the structural evolution of the fracture plugging layer under pressure. As to the formation mechanism of plugging layer, Yao et al. (2014, 2020) reported that microspheres could undergo five different migration and retention modes, such as surface deposition, smooth passage, direct interception, deformation migration, and rigid plugging, inside porous media. Song et al. (2018) reported that when the fracture width is smaller than or close to the particle size, the particle gel migrates along the fracture like a piston. Moreover, when the fracture width is larger than the particle size, gravity dominates the migration of the gel. The above studies mainly focus on the flexible particles in porous media and fractures; however, there are limited studies on plugging layers formed by water/oil-absorbing material, especially for lost circulation control of oil-based drilling fluid.

Many previous works on oil-absorbing gels have been conducted, but most of them focused on oil spill recovery or oily wastewater treatment, not on lost circulation control. Gels used for lost circulation control not only need to have good oil absorption performance, but also need to maintain high gel strength after oil absorption, while gels applied for treating oil spill and oily wastewater only need to have high oil absorption capacity (Zhang et al., 2019; Gautam et al., 2022). Although some oil-absorbing gels have been studied for lost circulation control, they were prepared either using rigid chain monomers to pursue gel strength or flexible chain monomers to pursue gel flexibility. Zhong et al. (2018) prepared a swellable polymer microgel using butyl methacrylate, methyl methacrylate and lauryl methacrylate. The microgel exhibits good deformability and compressibility after oil absorption, but it was not suitable for plugging large-scale fractures. Qiu et al. (2022) synthesized an oil-based gel with high structural strength and strong thermal stability using methacrylate and butyl acrylate, but its deformability was weak and it was not suitable for plugging while drilling.

In this study, an oil-absorbing gel with good gel strength, excellent flexibility, and oil absorption capacity for lost circulation control while drilling in fractured formations was synthesized using rigid and flexible chain monomers simultaneously. Moreover, the migration, accumulation, and filling mechanism of the oil-absorbing gel in visualized three-dimensional fractures were studied. Furthermore, the evolution characteristics of the strong and weak force chains in gel plugging layer were clarified. This work can provide a reference for future studies on lost circulation materials and lost circulation mechanism for oil-based drilling fluids in fractured formations.

2. Experimental

2.1. Materials

Butyl acrylate (purity ≥98%), sodium-*p*-styrenesulfonate (purity ≥90%), polyvinyl alcohol (purity ≥98%), and ethyl acetate (purity ≥99%) were purchased from Shanghai Aladdin Biochemical Co., Ltd. Octadecyl methacrylate (purity ≥98%), benzoyl peroxide (purity ≥90%), and divinylbenzene (purity ≥95%) were purchased from Shanghai Macklin Biochemical Co., Ltd. Flexible polyamide fiber with an average diameter of 66 μm, an average length of 3 mm, and a melting point of 280 °C was provided by Guangzhou ES Fiber Co., Ltd. Diesel was purchased from Shandong Juxin New Material Co., Ltd., and its basic parameters are shown in Table 1.

2.2. Synthesis of oil-absorbing gel

The synthesis procedure for the oil-absorbing gel is shown as

Table 1
Basic parameters of diesel.

Appearance	Density @ 20 °C, g/cm^3	Kinematic viscosity @ 40 °C, mm^2/s	Flash point, °C	Pour point, °C
Light, yellow, viscous liquid	0.845	3.8	81	4
Sediment content, wt%	Water content, wt%	Aromatics content, wt%	Sulfur content, wt%	Acid value, mg KOH/g
0	0	34.3	0.08	0.008

follows: (a) Dispersion preparation: 0.3 g of polyvinyl alcohol (dispersant) was added to 100 mL of deionized water, and the mixture was heated to and kept at 85 °C under stirring until complete dissolution. The mixture was then cooled to room temperature (25 °C) to obtain solution A. (b) Preparation of mixed monomer solution: 13 g of butyl acrylate (flexible chain monomer) and 34 g of octadecyl methacrylate (flexible chain monomer) were mixed in a beaker and stirred for 1 h at room temperature. Thereafter, 0.15 g of divinylbenzene (crosslinker), 10 g of ethyl acetate (pore-expanding agent), and 10.3 g of sodium-*p*-styrenesulfonate (rigid chain monomer) were subsequently added to the mixture and stirred thoroughly to obtain solution B. (c) Bulk gel preparation: Solution B was added to solution A and well-mixed under stirring, and 0.3 g of flexible fiber (toughener) was then added to the mixture and heated to 60 °C under continuous stirring. Thereafter, 0.1 g of benzoyl peroxide (initiator) was added to the mixture and heated to 90 °C, and a gel was obtained after 8 h. (d) Gel particle preparation: The gel was cooled to room temperature and washed three times with deionized water to remove unreacted chemicals. After that, the gel was dried under vacuum at 60 °C for 48 h. Then, it was crushed into the gel of different particle sizes and screened by sieves.

2.3. Oil absorption capacity test

The oil-absorbing gel with the required particle size and mass was dispersed in diesel, and left still for a certain time at a required temperature. Then gel was taken out to remove the excess oil from the surface, and the mass of the gel after oil absorption was weighed. Then the oil absorption capacity was calculated with the following equation to evaluate the oil absorption capacity of the gel.

$$Q = (m_2 - m_1)/m_1 \quad (1)$$

where m_1 is the initial mass of the gel, g; m_2 is the final mass of the gel after oil absorption, g; Q is the oil absorption capacity of the gel, g/g.

2.4. Microstructure characterization

The surface microstructure of the gel was observed with a cryofield emission scanning electron microscope, and the microstructure was characterized under different magnifications using the electron microscope. The infrared spectrum of the gel was analyzed using the Fourier transform infrared spectroscopy (FTIS) with the wavenumber varying from 500 to 4500 cm^{-1}, the number of scans is 4–32 times per millisecond.

2.5. Plugging performance test

A high-temperature and high-pressure fracture plugging simulation device was used (Fig. 1) to evaluate the plugging performance of the gel. The main experimental steps are as follows: (1) The temperature of the simulator was adjusted to the required. (2) A steel fractured core module with a certain fracture width was placed in the core holder, and a confining pressure was applied. (3) The diesel was injected into the fractured core at a rate of 2 mL/min until the fractured core was filled with diesel. (4) The oil-absorbing gel with required particle size and concentration was dispersed in the diesel to prepare the gel fluid. (5) The liquid was injected into the fractured core at a rate of 2 mL/min, and the injection pressure was recorded simultaneously. (6) When the flow of gel fluid from the fracture outlet stopped, the diesel was injected into the fractured core at the rate of 2 mL/min again while recording the injection pressure. Furthermore, the maximum injection pressure was determined as the bearing pressure capacity of the oil-absorbing gel.

2.6. Visualized fracture plugging experiment

The migration, accumulation, and filling morphology of the oil-absorbing gel in the fracture were observed using a visualized fracture plugging simulation device (Fig. 2). The main experimental steps are as follows: (a) A visualized fracture model as shown in Fig. 3 with entrance and exit widths of 1 and 0.5 mm, respectively, was fixed on the holder. (b) Diesel was injected into the model at a rate of 0.5 mL/min to fill the fracture. (c) The gel with required particle size and concentration was dispersed in the diesel to prepare the oil-absorbing gel fluid. (d) The fluid was injected into the model at a rate of 0.5 mL/min. Their migration, filling, and accumulation states in the fracture were recorded in real-time using an electron microscope. (e) After the fracture was completely filled by the gel, it was left to stand for a certain time period for the gel to completely absorb the oil and swell. (f) The gel fluid was placed with the diesel, which was continuously pumped into the fracture to observe the destabilization process of the gel plugging layer.

3. Performance evaluation of oil-absorbing gel

Oil absorption is one of the important properties of the oil-absorbing gel. First, the microstructure of the oil-absorbing gel was observed. Second, the effects of time, temperature, and particle size on the oil absorption capacity of the gel were studied. Finally, the plugging performance of the gel with combinations of different particle sizes and concentrations was evaluated to study the bearing pressure capacity of the gel for fractures of different widths. This study provides a reference for lost circulation control using the oil-absorbing gel in fractured formations.

3.1. Molecular structure characterization

The reaction mechanism of the oil-absorbing gel was analyzed and the schematic diagram of crosslinking reaction is shown in Fig. 4. The oil absorption capacity of the gel is mainly affected by types and concentrations of monomer, crosslinker, and initiator. The butyl acrylate, long chain octadecyl methacrylate with flexible chains were used to enhance the hydrophilic properties of the gel. The sodium-*p*-styrenesulfonate containing benzene ring group was used as the rigid part of the molecular chain to enhance the strength of gel structure. During the reaction, the butyl ester groups in butyl acrylate reacted with the octadecyl ester groups in octadecyl methacrylate to generate a crosslinking structure. Under the

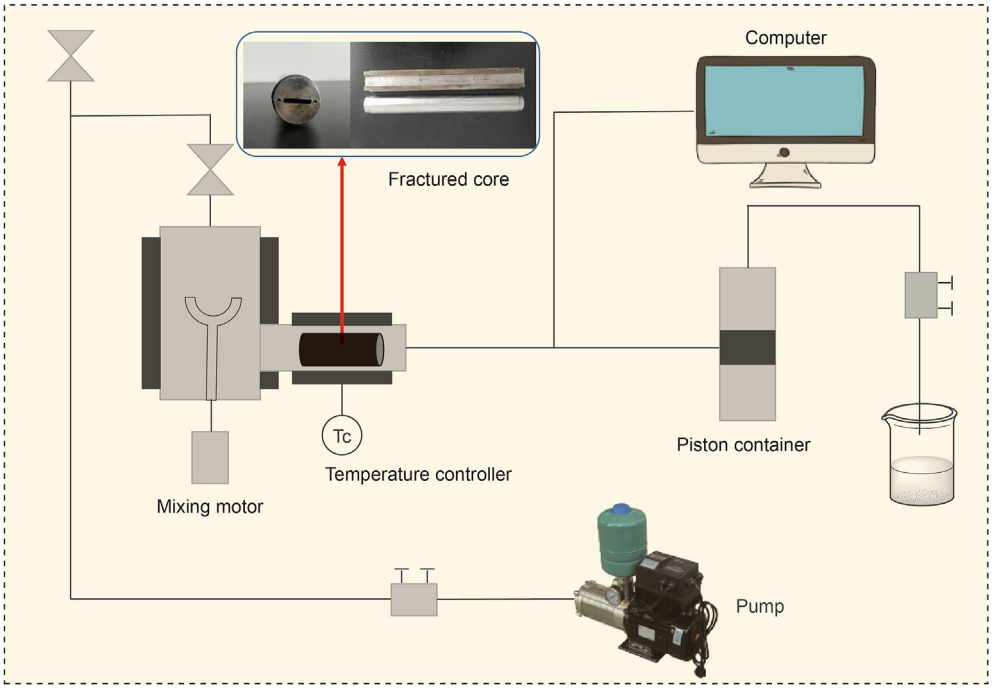

Fig. 1. High temperature and high pressure simulation device for fracture plugging.

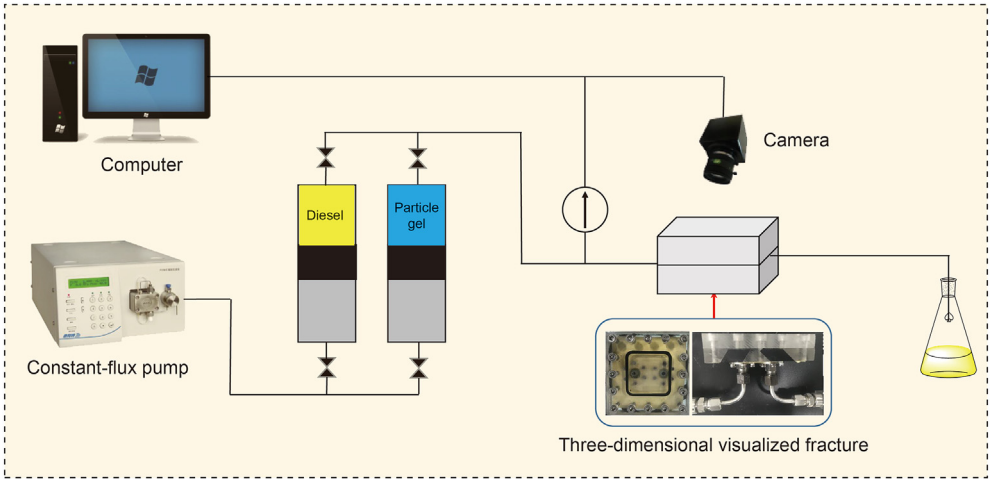

Fig. 2. Visualized simulation device for fracture plugging.

action of benzoyl peroxide, the sodium-*p*-styrenesulfonate and divinylbenzene reacted with the butyl acrylate/octadecyl methacrylate crosslinking structure through the polymerization among the methylene groups to form a three-dimensional network structure. Ethyl acetate was added during the polymerization to promote the formation of pores in the gel structure, which increased the oil-absorbing properties of the gel.

The infrared spectrum of the oil-absorbing gel was achieved to analyze its molecular structure with a wavenumber range of 500–4500 cm^{-1}, and the result is shown in Fig. 5. The absorption peak at 3403 cm^{-1} represents the stretching vibration of C–H on unsaturated carbon (double bonds and benzene), the absorption peak at 2933 cm^{-1} is the stretching vibration of C–H on saturated carbon (methyl and methylene groups), the absorption peak at 1741 cm^{-1} is associated with the stretching vibration of C=O in ester group (Du et al., 2018). Moreover, the absorption peaks at 1451 and 1298 cm^{-1} represent the bending vibration in C–H plane and the stretching vibration of C–O in ester group, and the peak at 1041 cm^{-1} is correlated with the characteristic in-plane rocking vibration of CH_2 in the long-chain alkyl group (octadecyl). In addition, the peak at 625 and 549 cm^{-1} reflect the monosubstituted benzene ring. Results show that butyl acrylate, sodium-*p*-styrenesulfonate, octadecyl methacrylate and divinylbenzene were involved in the structure of the oil-absorbing gel.

3.2. Microstructure characterization

The microstructures of the oil-absorbing gel at different magnifications are shown in Fig. 6. There are many pores with different sizes on gel microstructure because not all groups or segments (e.g., $-CH_2-CH_2-$) on gel molecular chains can be crosslinked, and that's what gels have in common (Sauerwein and Steeb, 2020). Pores

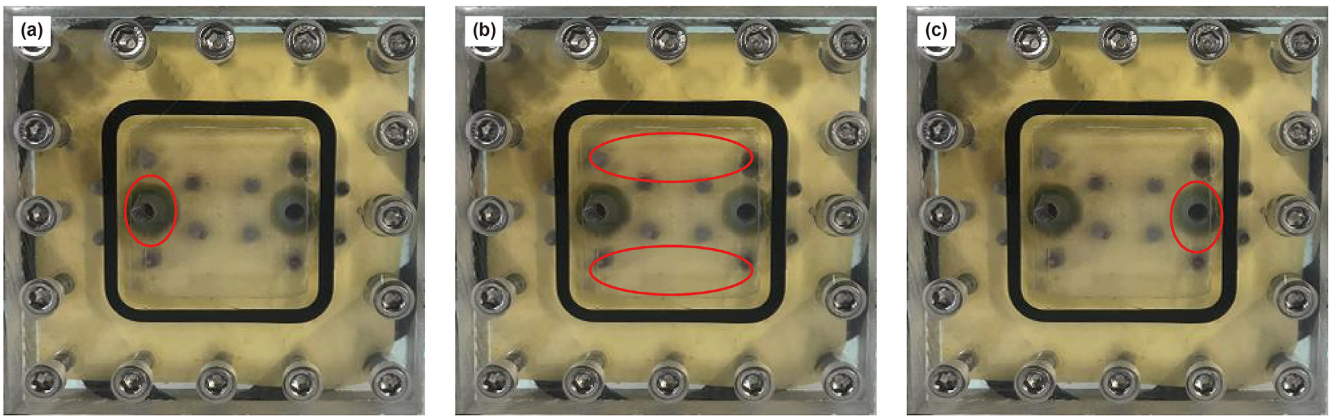

Fig. 3. Pictures of visualized fracture model. (**a**) Fracture entrance; (**b**) fracture top and bottom; (**c**) fracture exit.

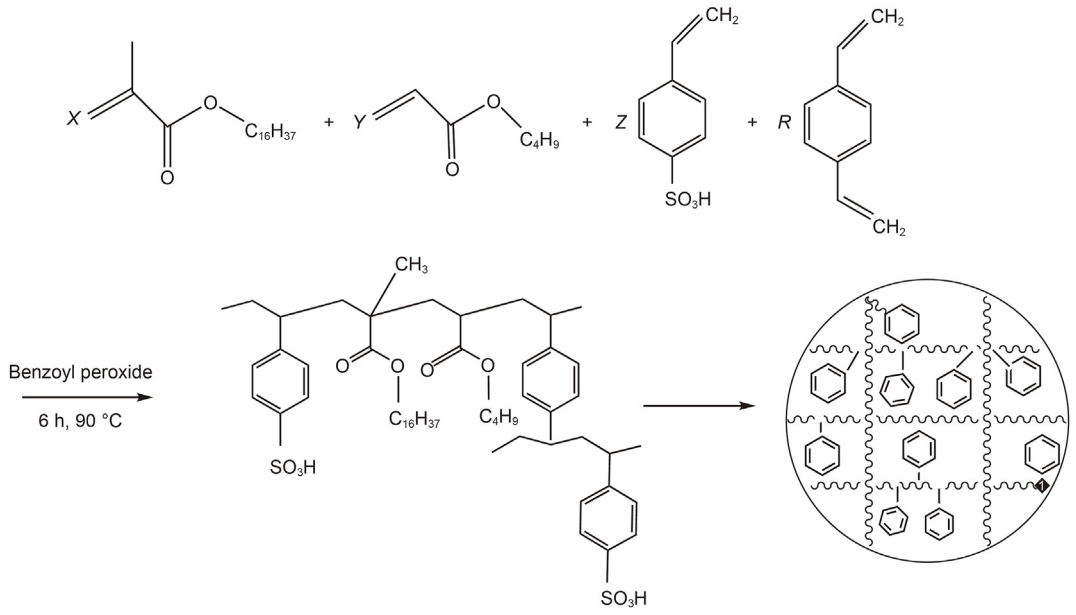

Fig. 4. Schematic diagram of oil-absorbing gel synthetic reaction.

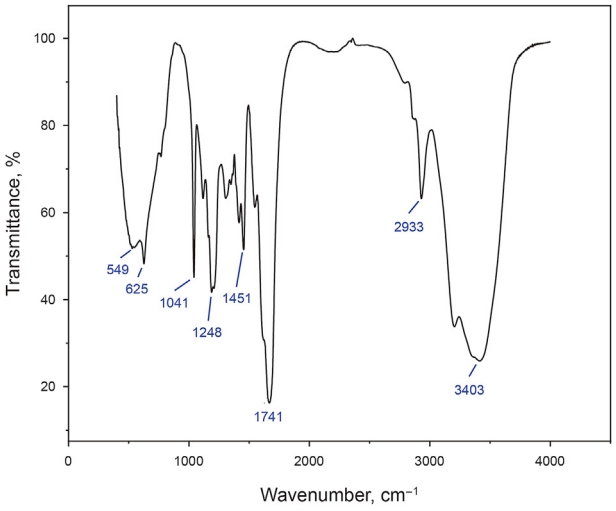

Fig. 5. Infrared spectrum of the oil-absorbing gel.

serve to store oil molecules after oil absorption. The formation of wrinkles on gel surface is attributed to different crosslinking reactions among components. The elastic structure of the gel is formed by the reaction between flexible chain monomers such as butyl acrylate and long chain octadecyl methacrylate, and reactions between monomers containing benzene ring produce the rigid structure of the gel. After the removal of tensile force, the self-wrinkling on gel surface occurs because of the different modulus of rigid structure and elastic structure (Lei et al., 2019). This effectively enlarged the specific surface area of the gel and the contact area between the gel and oil molecules. The microscopic image with a magnification of 10,000 (Fig. 6f) reveals the presence of many irregular lamellar structures on the gel surface. Moreover, the pores were mainly distributed between the irregular lamellar structures; hence, the oil storage space was significantly improved. Meanwhile, the capillary force of micropores is conducive to improving the absorption capacity, and the oil molecules do not likely spill out after absorption, thereby exhibiting good oil storage performance. Fig. 7 shows the schematic of the oil absorption mechanism of the gel. First, the gel adsorbs oil molecules on the surface through capillary force, and many oil molecules enter the

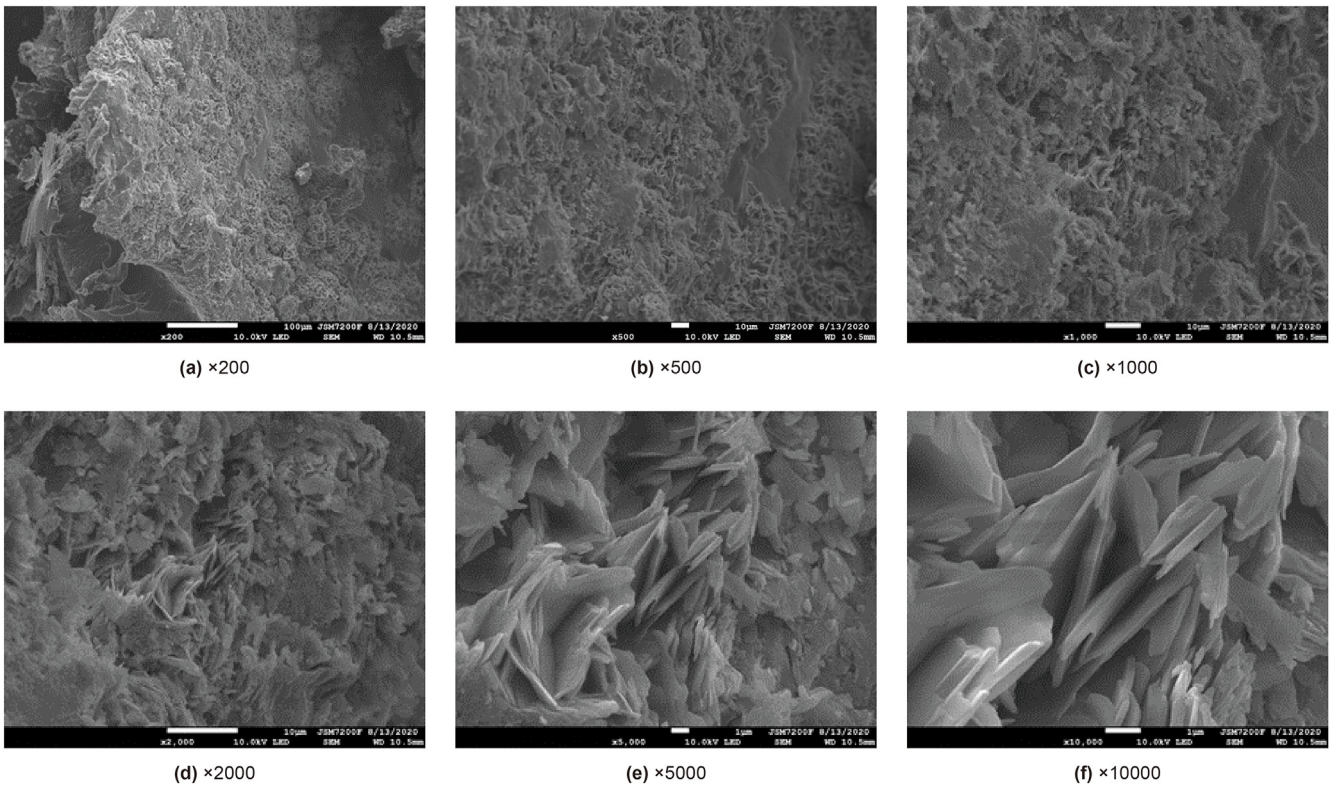

Fig. 6. Microstructure of oil-absorbing gel at different magnifications.

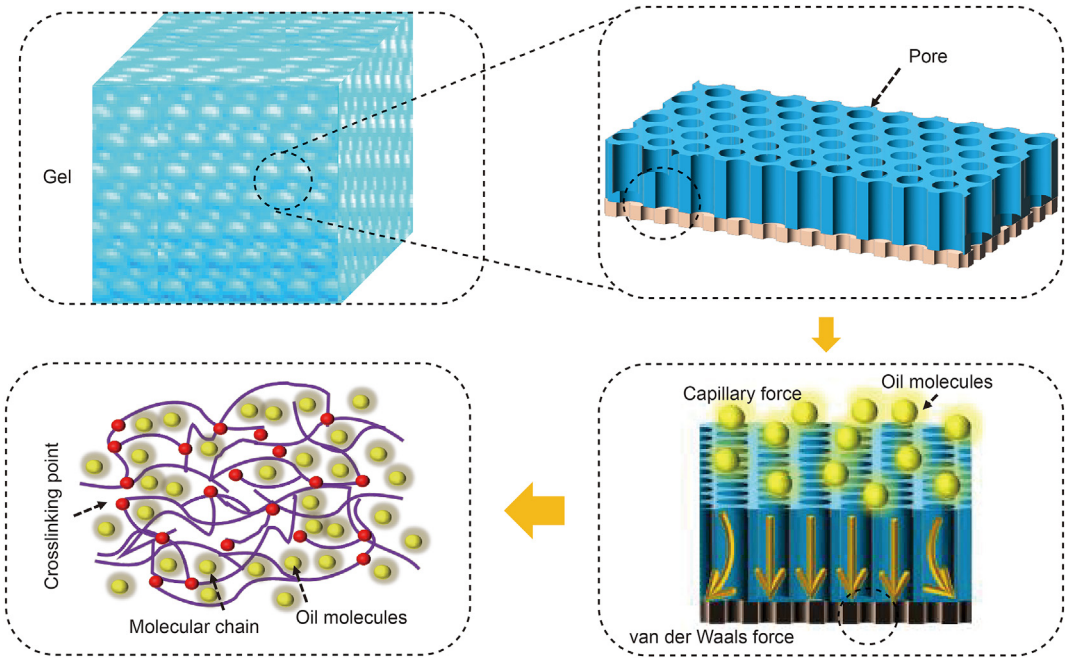

Fig. 7. Schematic diagram of oil absorption process of gel.

internal space of the three-dimensional structure of the gel through surface micropores. Thereafter, solvation effect occurs between the molecular chain segments with lipophilic groups (e.g., long-chain alkyl groups and benzene ring groups) and the oil molecules, gradually stretching the molecular chain segments (Kundu and Mishra, 2013; Yu et al., 2021). At the same time, the outer surface wrinkles and the large internal space have an excellent covering effect on the oil molecules, which offers good oil absorption capacity to the gel (Zhang et al., 2017).

3.3. Oil absorption capacity of gel

The gel absorbs oil and swells upon entering the drilling fluid loss channel, thereby increasing the particle size to immediately plug the formation with lost circulation. The oil absorption capacity of the gel is influenced by various factors such as time, temperature, and particle size.

3.3.1. Effect of time

The oil absorption process of the gel is essentially the process of adsorption and diffusion of small oil molecules on the porous structure of the gel. Based on the mechanism, the adsorption can be divided into two categories: physical adsorption and chemical adsorption. Physical adsorption is mainly induced by van der Waals force, while chemical adsorption mainly includes chemical bonding. To study the adsorption mechanism of oil molecules on gel and explain the oil absorption capacity of the gel at different times (Chen et al., 2020), a kinetic model was used to describe the kinetic oil absorption behavior of the gel (Alves et al., 2017; Ho and McKay, 1999).

3.3.1.1. Lagergren pseudo-first-order model. Lagergren pseudo-first-order model assumes that the adsorption rate of oil molecules is proportional to the number of unoccupied sites by oil molecules. The kinetic equation is:

$$\ln(Q_e - Q_t) = \ln Q_e - k_1 t$$

where Q_e is the equilibrium oil absorption capacity, g/g; Q_t is the oil absorption capacity at time t, g/g; and k_1 is the first-order oil adsorption rate constant, min^{-1}. The parameters Q_t and k_1 can be obtained by plotting time t against Q_e.

3.3.1.2. Lagergren pseudo-second-order model. According to the Lagergren pseudo-second-order model, the adsorption rate depends on the concentration of oil molecules and the active sites on the gel. The physical interpretation of this model is that the driving force of the adsorption process depends on the number of active sites available. The kinetic equation of this model is:

$$\frac{t}{Q_t} = \frac{1}{k_2 Q_e^2} + \frac{t}{Q_e}$$

where k_2 is the second-order oil adsorption rate constant, g/(mg min). The parameters Q_t and k_2 can be obtained by plotting t against Q_e.

In this study, a certain mass of dry gel with an average particle size of 0.3 mm was weighed and dispersed in diesel. The gel was sampled every hour, and the excess oil was removed from the surface using an oil-absorbing sheet. The oil absorption capacity of the gel at different times was recorded, and the test was run for 7 h. The variation in the oil absorption capacity of the gel was fitted with the Lagergren pseudo-first-order and Lagergren pseudo-second-order kinetic equations. The experimental and fitting results are shown in Fig. 8 and Table 2.

As shown in Fig. 8, the oil absorption capacity of the gel was fast in the initial stage, reaching 2.9 g/g in 3 h. After 3 h, the oil absorption capacity of the gel gradually slowed down, and a peak value of 4.34 g/g was achieved in 7 h. The oil molecules entered the pores under the action of capillary force after meeting the gel, and this molecular diffusion mainly determined the oil absorption capacity. At this time, only a small amount of oil molecules reached the internal structure, and the polymer structural units with lipophilic groups were not fully stretched, thereby resulting in a slow oil absorption capacity. With the increase in time, many oil molecules met the gel and entered the internal structure of the gel through the pores. Under the action of the van der Waals force, solvation occurred between the internal lipophilic groups and oil molecules. In this case, the factor determining the oil absorption capacity of the gel shifted from molecular diffusion to thermodynamics. Moreover, solvation fully stretched the internal macromolecular chain segments, resulting in a rapid increase in the oil absorption capacity of the gel (Deng et al., 2015; Rong et al., 2017). As oil molecules continuously entered the gel internal structure and filled the pore space, the diffusion coefficient of the oil molecules gradually decreased. At this time, the oil absorption capacity was mainly controlled by kinetics and decreased gradually. With the accumulation of oil molecules, the three-dimensional network structure of the gel stretched continuously. The stretching between covalent bond crosslinking points reduced the conformational entropy, and the retractive force generated at the crosslinking points caused elastic retraction of the chain segments. Then, the molecules reached thermodynamic equilibrium, and the oil absorption capacity decreased continuously to reach the absorption equilibrium (Deng et al., 2020). The oil absorption capacity at different time points was fitted with the Lagergren pseudo-first-order and Lagergren pseudo-second-order models, and the fitting parameters are shown in Table 1. The determination coefficient (R^2) obtained from the fitted curves of the first-order and the second-order kinetic equations were 0.99 and 0.98, respectively. Compared to the fitting results obtained from the first-order equation, the theoretical saturated oil absorption Q_e determined by fitting the experimental results with the second-order equation deviated more from the experimental value, indicating that the Lagergren pseudo-first-order kinetic equation is more suitable for describing the oil absorption capacity of the gel at different times.

3.3.2. Effect of temperature

The oil-absorbing gel with an average particle size of 0.3 mm was dispersed in diesel and sealed at 25, 110, 120, 130, and 140 °C. The reason for choosing 25–140 °C as experimental temperatures is that the gel was degraded and the oil absorption capacity cannot be determined at 150 °C. The effect of temperature on the oil absorption capacity of the gel was evaluated using the mass ratio before and after oil absorption.

The fitting results of the oil adsorption kinetics of the gel at different temperatures are shown in Fig. 9, and the model parameters are listed in Table 3. Results indicate that the absorption capacity of the gel was rapid in the initial stage under all temperatures and gradually decreased after 3 h, and it gradually approached the equilibrium level in approximately 7 h. Moreover, the initial oil absorption capacity of the gel accelerated with increasing temperature, accompanied by a gradual increase in oil absorption capacity. The oil absorption capacity of the gel increased up to 20.93 g/g at 140 °C, suggesting that higher temperatures are favorable for the forward reaction (Sokker et al., 2011). The oil absorption process of gel is mainly driven by molecular diffusion and thermodynamic driving force. In addition, the final oil absorption capacity of the gel is mainly determined by the van der Waals force between oil molecules and the gel structure and the gel crosslinking density. With the increase in temperature, the oil molecules became active gradually, the molecular diffusion coefficient increased, and the solvation between oil molecules and the internal lipophilic chain segments of the gel improved (Bai et al., 2018). At the same time, higher temperatures result in faster diffusion of oil molecules from the molecular surface into the gel structure. In addition, temperature elevation leads to the destruction of the crosslinking points formed via hydrogen bonds. The intermolecular force is weakened and the number of hydrogen bond crosslinked points inside the gel is reduced. Therefore, the crosslinking density

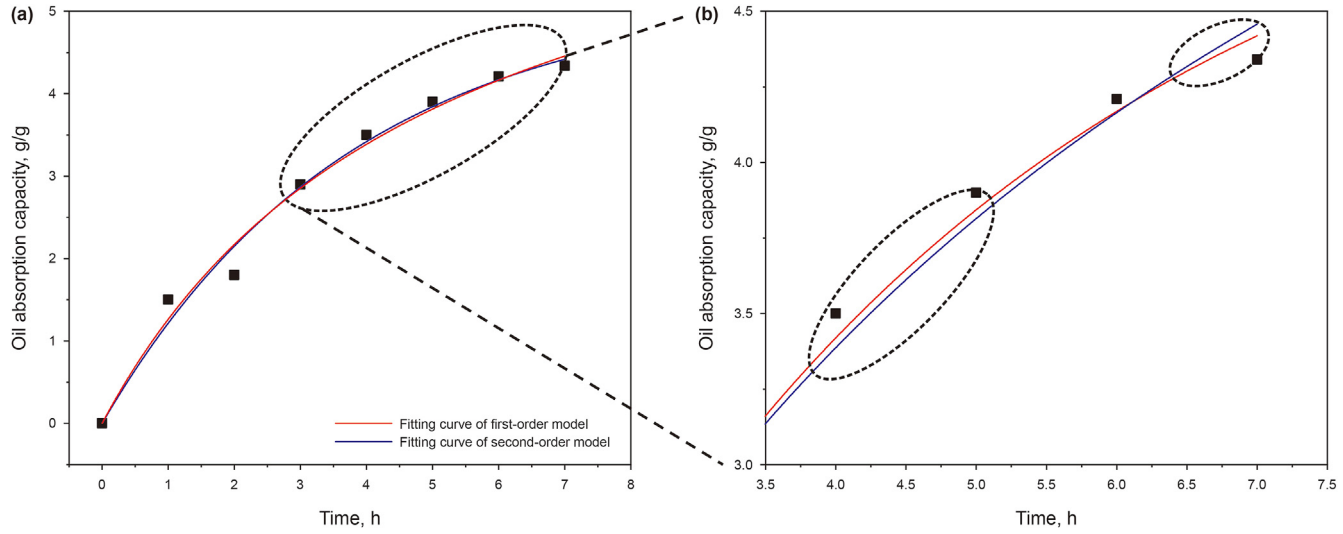

Fig. 8. Fitting results of Lagergren pseudo-first-order and second-order models of oil-absorbing gel at different times.

Table 2
Fitting results of adsorption kinetics of oil-absorbing gel in diesel at different times using Lagergren pseudo-first-order model and Lagergren pseudo-second-order model.

Model	Fitting equation	Equilibrium oil absorption capacity Q_e, g/g		R^2
		Theoretical value	Actual value	
Lagergren pseudo-first-order model	$Q_e = Q_t - \exp(\ln Q_t - kt)$	4.40	4.34	0.99
Lagergren pseudo-second-order model	$Q_e = t/[(1/(kQ_t^2)) + t/Q_t]$	4.46	4.34	0.98

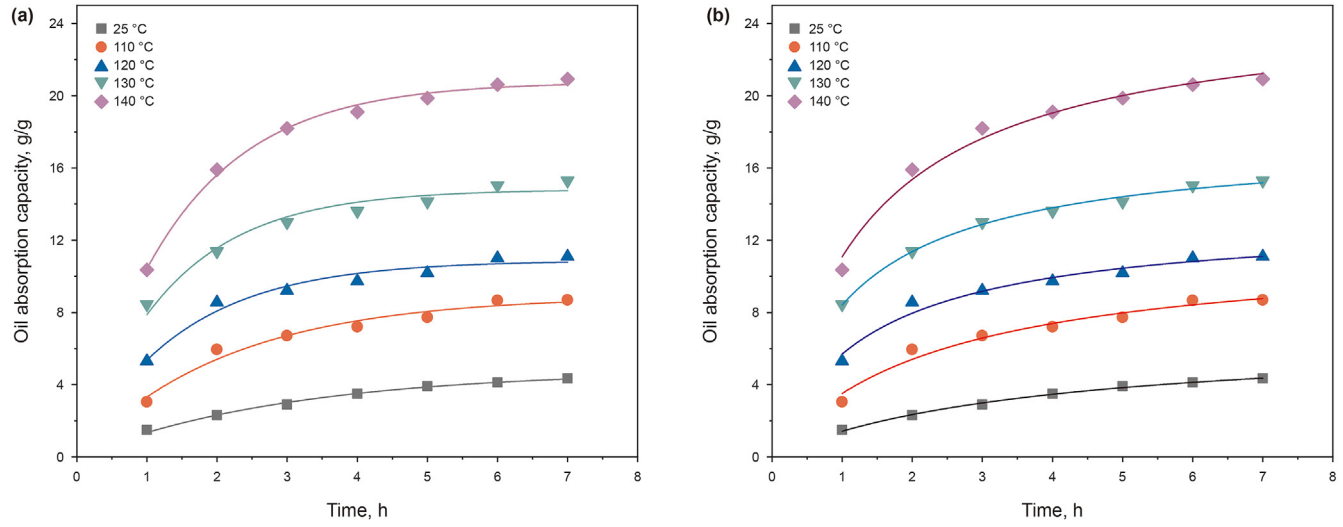

Fig. 9. Fitting results of adsorption kinetics of oil-absorbing gel at different temperatures. (**a**) Fitting result of Lagergren pseudo-first-order model; (**b**) fitting result of Lagergren pseudo-second-order model.

of the gel decreases, and the internal molecular lipophilic chain segments stretch, leading to volume expansion and larger space between molecular chain segments. Meanwhile, the movement velocities of branched chains, side chains, and the whole molecules are accelerated with increasing temperature because that the molecular chains are in the activated state (Yang et al., 2021). Upon temperature elevation, the combined effects of the activated molecular chain and the increased movement velocity increased the oil absorption capacity of the gel. It is specifically shown that when the temperature increases, the oil molecules continuously enter the gel under the action of van der Waals force and fill the network structure, the oil absorption capacity accelerates and increases, as shown in Fig. 10. The theoretical saturated oil absorption Q_e determined by the Lagergren pseudo-second-order kinetic equation is very close to the experimental value with the determination coefficient (R^2) of 0.97–0.99, compared to that determined by the Lagergren pseudo-first-order kinetic equation, indicating that the Lagergren pseudo-second-order kinetic equation accurately describes the oil absorption capacity of the gel at different temperatures.

Table 3
Fitting results of adsorption kinetics of oil-absorbing gel in diesel at different temperatures using Lagergren pseudo-first-order model and Lagergren pseudo-second-order model.

Model	Temperature, °C	Fitting equation	Equilibrium oil absorption capacity Q_e, g/g		R^2
			Theoretical value	Actual value	
Lagergren pseudo-first-order model	25	$Q_e = Q_t - \exp(\ln Q_t - kt)$	4.34	4.34	0.99
	110		8.57	8.69	0.97
	120		10.78	11.09	0.97
	130		14.74	15.30	0.96
	140		20.6	20.93	0.99
Lagergren pseudo-second-order model	25	$Q_e = t/\left[\left(1/\left(kQ_t^2\right)\right) + t/Q_t\right]$	4.34	4.34	0.99
	110		8.76	8.69	0.97
	120		11.1	11.09	0.97
	130		15.17	15.30	0.99
	140		21.23	20.93	0.98

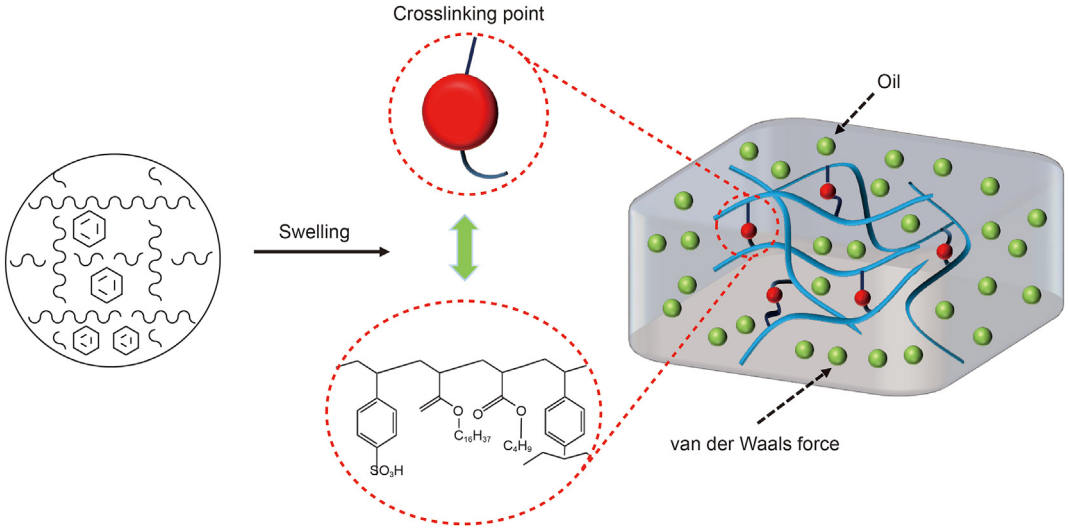

Fig. 10. Schematic diagram of oil absorption mechanism of oil-absorbing gel.

3.3.3. *Effect of pressure*

The oil-absorbing gel with an average particle size of 0.3 mm was dispersed in diesel and sealed in ageing cans at different pressures of atmospheric pressure (0.1 MPa), 1.0, 3.0, and 5.0 MPa, respectively. The effect of pressure on oil absorption capacity of the gel was investigated and the data were plotted in Fig. 11. Results show that although the oil absorption capacity of the gel continued to increase with the extension of time, the effect of pressure on the final oil absorption capacity (about 4.30 g/g) was slight under the same conditions. However, the oil absorption process of gel is different under different pressure conditions. At atmospheric pressure, the oil absorption capacity reached 3.50 g/g after 5 h, it decreased to 3.42, 3.33, and 3.21 g/g at 1.0, 3.0, and 5.0 MPa, respectively. The internal and external pressures of the gel are the same in a tight space with unlimited boundary, and the oil adsorption process of the gel is mainly controlled by the properties of gel itself, contributing to the final oil absorption capacity under different external pressures. However, when the gel is placed in a space with limited boundary such as pores or fractures, the final oil absorption capacity decreases with the increase in external pressures. Cohen and McMeeking (2019) studied the swelling induced microstructure of gels by employing a Langevin-based microscopically motivated model, and pointed out that two conditions were required to achieve an equilibrium configuration of swelling gels in a liquid solvent at given but different pressures. From the mechanical viewpoint, the gel must satisfy mechanical equilibrium and comply with the mechanical boundary conditions, and from the chemical viewpoint, the chemical potential of liquid solvent molecules in gels and in external solvent must be equal. The simulation results are consistent with the conclusion of this study.

3.3.4. *Effect of particle size*

Dried oil absorbing gel with particle sizes of 0.2. 0.3, and 0.6 mm was dispersed in the diesel to evaluate the oil absorption capacity of the gel with different sizes using the mass ratio before and after oil absorption.

The change in oil absorption capacity and fitting results of the gel with different particle sizes with respect to time is shown in Fig. 12, and the model parameters are listed in Table 4. In the initial stage, the oil absorption capacity of the gel with an average particle size of 0.2 mm was the fastest. Thereafter, the oil absorption capacity slightly decreased in 1–2 h, reaching 4.38 g/g in 2 h. The oil absorption capacity of the gel gradually stabilized in 2–6 h and saturated to 4.78 g/g after 6 h. The gel with an average particle size of 0.3 mm exhibited a fast oil absorption rate in 0–1 h, and the corresponding oil absorption capacity after 2 h was 3.58 g/g. In the time interval of 2–5 h, the oil absorption capacity of the gel (0.3 mm) decreased continuously. The gel with an average particle size of 0.6 mm also exhibited a rapid oil absorption rate in 0–1 h, and the oil absorption capacity of the gel reached 3.07 g/g after 2 h.

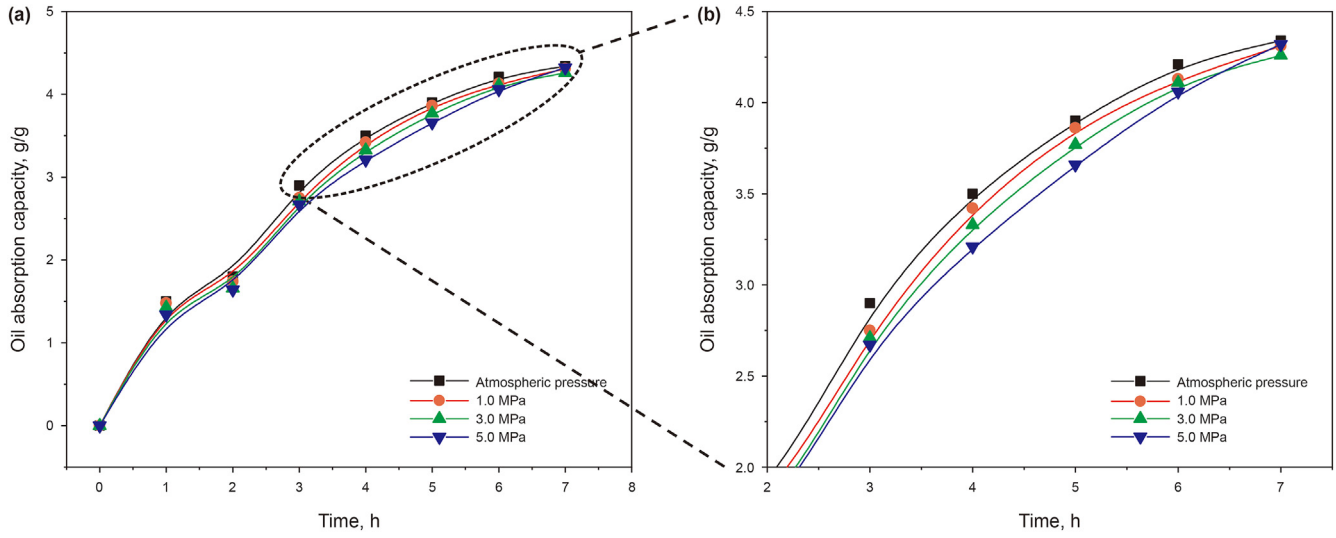

Fig. 11. Effect of pressure on oil absorption property of oil-absorbing gel.

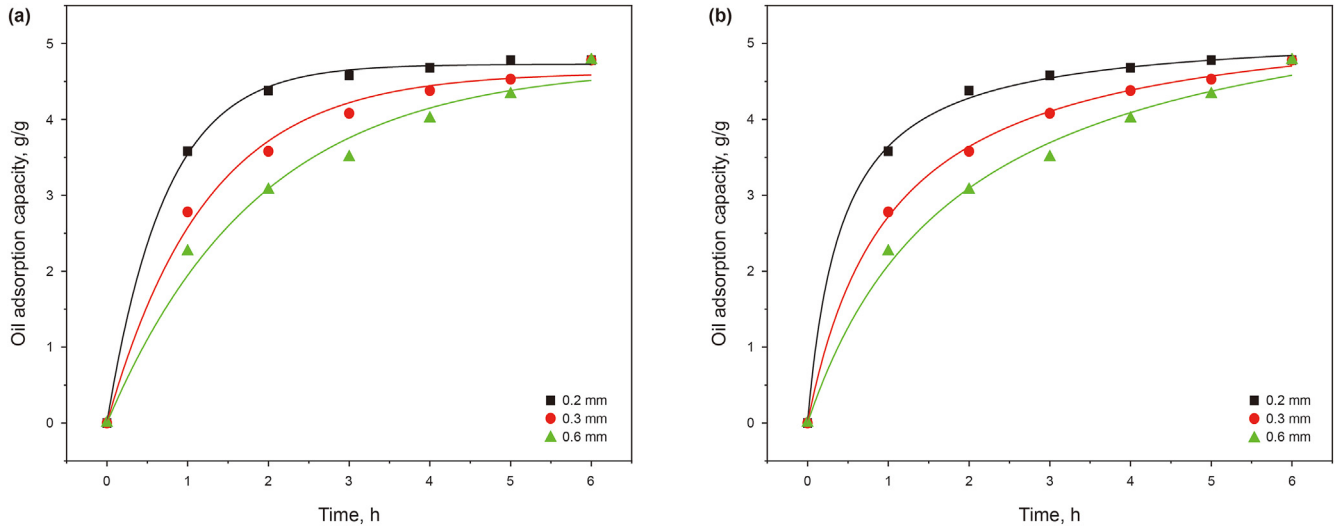

Fig. 12. Oil absorption capacity evolutions and fitting results of adsorption kinetics of oil-absorbing gel with different particle sizes. (**a**) Fitting result of Lagergren pseudo-first-order model; (**b**) fitting result of Lagergren pseudo-second-order model.

Table 4
Fitting results of adsorption kinetics of oil-absorbing gel in diesel with different particle sizes using Lagergren pseudo-first-order model and Lagergren pseudo-second-order model.

Model	Particle size, mm	Fitting equation	Equilibrium oil absorption capacity Q_e, g/g		R^2
			Theoretical value	Actual value	
Lagergren pseudo-first-order model	0.2	$Q_e = Q_t - \exp(\ln Q_t - kt)$	4.68	4.78	0.99
	0.3		4.58	4.78	0.99
	0.6		4.50	4.78	0.98
Lagergren pseudo-second-order model	0.2	$Q_e = t/\left[\left(1/\left(kQ_t^2\right)\right) + t/Q_t\right]$	4.79	4.78	0.99
	0.3		4.68	4.78	0.99
	0.6		4.58	4.78	0.99

Thereafter, the oil absorption capacity slightly decreased in 2–6 h; however, the overall oil absorption capacity still increased during this interval. As shown in Fig. 12, the particle size significantly influences the oil absorption process of the gel. That is, as the particle size increases, the oil absorption capacity of the gel becomes slow at first. This is because oil absorption is essentially the diffusion process of oil molecules from the outer surface to the gel interior, and different particle sizes result in different migration distances of the oil molecules under the same conditions. The larger the particle size, the longer is the migration distance from the gel surface to the

interior. In addition, large particle gel forms a dense layer of oil molecules due to surface expansion, resisting the oil molecules from entering the interior of the gel (Bu et al., 2019). In contrast, small particle gel has a large relative surface area; therefore, the contact range between the oil molecules and the surface of the particles is large, and the molecular diffusion is rapid. In summary, the smaller the particle size, the faster is the oil absorption capacity in the same time period. Upon entering fractured formation, small particle gel can swiftly reach the absorbing equilibrium, and large particle gel has appropriate absorbing volume, effectively bridging and plugging the pores and fractures. The oil absorption capacity of the gel with different particle sizes were fitted with the Lagergren pseudo-first-order and Lagergren pseudo-second-order kinetic equations. According to Table 3, the theoretical saturated oil absorption (Q_e) determined by the Lagergren pseudo-second-order kinetic equation is very close to the experimental value with all the determination coefficients R^2 above 0.99 compared to that determined from the Lagergren pseudo-first-order kinetic equation, indicating that the Lagergren pseudo-second-order kinetic equation can accurately describe the oil absorption capacity of the gel with different particle sizes.

3.4. Plugging performance of gel

3.4.1. Plugging performance on porous media

To evaluate the plugging performance of the oil-absorbing gel, porous media with an average porosity of 47.2% and an average permeability of 28.6 μm^2 were applied. According to the core analysis, the average diameter of pores was about 0.6 mm. Because the matching relationship between particle size and pore size of plugging material is very important, many studied have been conducted to explore the optimal particle size and concentration of plugging material. The “one-third rule” (Abrams, 1997) is the earliest and commonly used principle for pore plugging, but it is mainly applicable to the temporary formation plugging with low plugging capacity. The “one-half rule” (Li, 2013) was an extension of the “one-third rule” and consider that the ideal packing effect can be easily achieved based on this rule. The equal diameter bridging rule has been also verified by many researchers (Xu et al., 2019; Li et al., 2022) and our previous study (Lei et al., 2022) when plugging large-scale pores and fractures. However, the above three rules apply primarily to rigid particles instead of elastic particle gel. To explore the matching relationship between elastic particle size and pore size, three rules were referred to in this study and eight formulae composed of the gel with particle size of 0.6, 0.3, and 0.2 mm, respectively, after oil absorption were applied based on the “one-third rule”, “one-half rule” and equal diameter bridging rule. The loss volume of liquids within 30 min was monitored at 100 psi and 140 °C. After the plugging tests, the remaining fluid in the simulation device was drained to obtain the filter cake, and actual images were taken. Thereafter, the optimal amount of added gel was determined, and the experimental results are shown in Figs. 13 and 14.

According to Fig. 13, the gel fluid was completely lost for formula 1#, formula 3#, formula 5#, and formula 7#. A fluid loss of 35, 46, 42, and 34 mL was recorded for combination formula 2#, formula 4#, formula 6#, and formula 8#, respectively. The lowest fluid loss amount was 34 mL in the case of formula 8#, which is the best plugging performance achieved among the combinations. Fig. 14 shows that small particle gel made gel filter cake smoother, and the gel filter cake becomes thinner when a formula with low concentrations of the gel combination. Moreover, fluid loss data reflect that to reduce the drilling fluid loss in porous media, the total concentration of the gel with different particle sizes should exceed 3%. In addition, the combination of the gel with three different kinds of particle sizes is conductive to reducing fluid loss. As shown in Fig. 14a, the particle gel flocculated, and the filter cake on the surface of porous media became very loose, resulting in a higher fluid loss volume. After compounding the gel of different particle sizes (Fig. 14h), the particles progressively filled up the pores. Moreover, the filter cake on the surface of porous media became smooth and dense, thereby reducing the fluid loss volume. Therefore, formula 8# was selected for subsequent testing.

3.4.2. Plugging performance on fractures

The high-temperature and high-pressure fracture simulator was used to evaluate the plugging performance of the oil-absorbing gel in fractures. Li et al. (2022) investigated the plugging effects of single-particle bridging and double-particle bridging in fractures and found that the double-particle bridging was more likely to fail under the action of particle collision and fluid erosion compared with the single-particle bridging. Xu et al. (2021) also reported a similar phenomenon. Therefore, only the equal diameter bridging theory was adopted to achieve the single-particle bridging in fractures. During the experiments, the gel with average particle sizes of 1.11, 2.16, and 3.80 mm after oil absorption was injected into the steel fractured cores (30 cm in length and 2.5 cm in diameter) with average entrance and exit widths of 2–10 mm and 1–7 mm, respectively. The gel concentration was 5%, and the bearing pressure capacity of the gel in fractures was tested at 140 °C. As shown in Table 5, the bearing pressure capacity of the oil-absorbing gel for fractures with average entrance and exit widths of 2 and 1 mm, 3 and 2 mm, 5 and 3 mm, and 7 and 5 mm were 7.67, 7.13, 6.72 and 4.29 MPa, respectively, demonstrating excellent plugging performance. However, with the entrance and exit widths increased to 10 and 7 mm, respectively, the bearing pressure capacity decreased to only 1.91 MPa. Data indicate that the oil-absorbing gel has good plugging performance on fractures with a width of less than 5 mm, which can meet most of the requirements of oil-based drilling fluid for lost circulation control while drilling.

To further prove the favorable properties of the oil-absorbing gel prepared in the present study, a kind of oil-absorbing material (ZDY, Sichuan Dedao Industrial Co., LTD) applied in oilfields has been used for comparison with this product. Oil absorption capacity and plugging performance of ZDY have been conducted under the same conditions with the oil-absorbing gel. Results show that the oil-absorbing gel shows better absorption capacity and higher bearing pressure capacity for porous media and fractures. According to the industrial product price of chemicals used to prepare the oil-absorbing gel and other production inputs, the cost needed to produce the gel is about 22,000 CNY per ton and its market price is 36,000 CNY per ton, which is obviously lower than that of ZDY of 44,000 CNY per ton.

3.4.3. Field test

The W-XXX well is a shale gas well in the Sichuan Basin. When the diesel-based drilling fluid was used to drill into the Longmaxi Formation with a temperature of 108 °C, the drilling fluid lost circulation with a loss rate of 14.6 m^3/h occurred. According to logging interpretation of adjoining wells, the Longmaxi Formation was characterized by fractures ranging from 0.05 to 1.18 mm in width. The oil-absorbing gel with an average size of 0.98 mm after oil adsorption and a concentration of 5% was added into diesel-based drilling fluid as the lost circulation material. After the drilling fluid carrying the gel was circulated twice in the wellbore, the loss rate of the drilling fluid decreased to 3.3 m^3/h. Therefore, the gel was added to the drilling fluid again to maintain its concentration at 5%, and then the drilling fluid was continually circulated in the wellbore. The lost circulation disappeared after twice circulation again of the diesel-based drilling fluid, indicating a successful lost

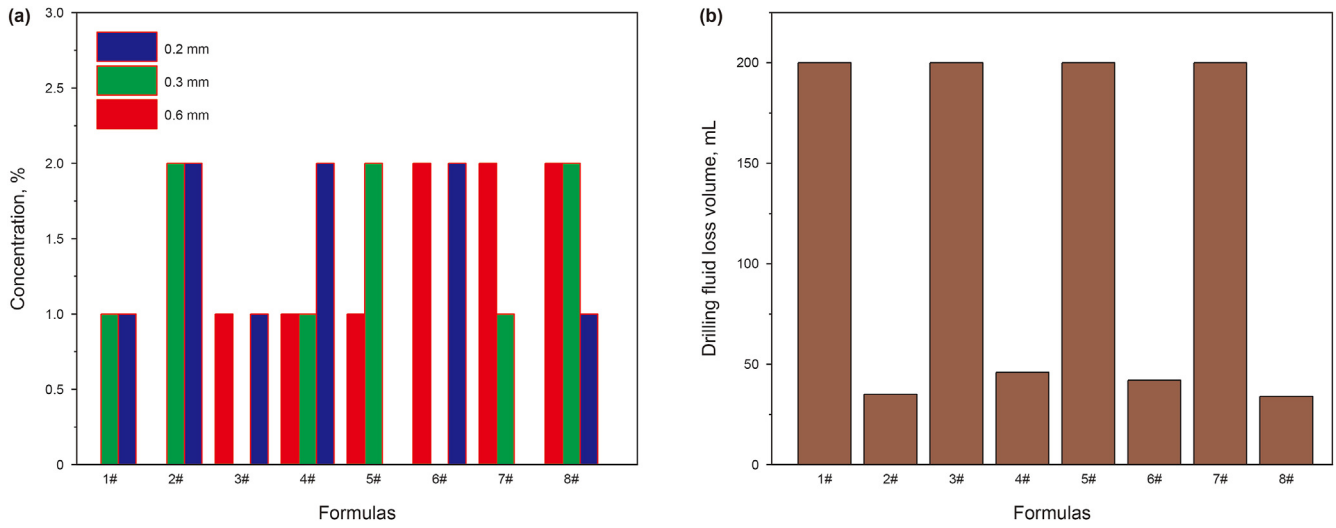

Fig. 13. Plugging performance of oil-absorbing gel for porous media. (**a**) Concentration composition of gel with different particle sizes in formulas; (**b**) drilling fluid loss volume after porous media plugging with the use of different gel formulas.

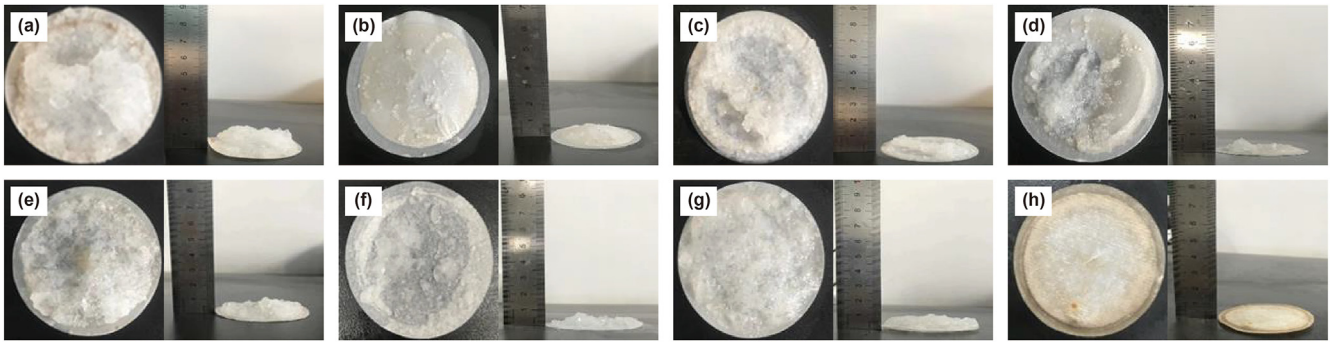

Fig. 14. Gel plugging layers formed by different gel formulas after porous media plugging. (**a**) Formula 1#; (**b**) formula 2#; (**c**) formula 3#; (**d**) formula 4#; (**e**) formula 5#; (**f**) formula 6#; (**g**) formula 7#; (**h**) formula 8#.

Table 5
Bearing pressure capacity of oil-absorbing gel for fracture at 140 °C.

No.	Width of fracture entrance, mm	Width of fracture exit, mm	Particle size, mm		Bearing pressure capacity, MPa
			Before oil adsorption	After oil adsorption	
1	2	1	0.457	1.112	7.67
2	3	2	0.957	2.164	7.13
3	5	3	1.680	3.809	6.72
4	7	5	1.680	3.809	4.29
5	10	7	1.680	3.809	1.91

circulation control of the oil-absorbing gel for fractured formation.

4. Microscopic plugging mechanism of oil-absorbing gel

Many studies have been conducted to explore the selection rules of types and particle sizes of lost circulation materials (Bai et al., 2021b; Kang et al., 2019). However, these studies mainly focus on optimizing lost circulation materials and investigating the corresponding mechanisms of rigid lost circulation materials (Yang et al., 2022). For fractured formations, there are limited studies on the dynamic plugging process of oil-absorbing materials with combinations of different particle sizes and on the structural instability mechanisms of the plugging layer.

4.1. Dynamic migration mechanism

To study the plugging process of oil-absorbing gel in fractures, based on the equal diameter bridging rule, blue particle gels with an average particle size of 0.5 mm after oil absorption were selected and dispersed in diesel with a concentration of 3%. Thereafter, the gel fluid was injected at the rate of 0.5 mL/min from the left side into the fracture visualization model with entrance and exit widths of 1 and 0.5 mm, respectively. Because natural fracture surfaces are normally rough surfaces and a completely smooth fracture surface does not exist, the fracture wall surface was polished and ground to simulate the real roughness. The migration pattern of the oil-absorbing gel through the fracture was observed using an electron microscope. The macroscopic migration process of the gel in

the fracture is shown in Fig. 15. The light-colored part of the image is diesel, which is applied to simulate oil-based drilling fluid and fills the fracture space at first, and the blue-part of the image is the particle gels dispersed in diesel.

From the macroscopic point of view, owing to the large width of the fracture, the migration of the gel in the fracture was affected by various forces such as inertia effect, diffusion and deposition, and gravitational settling (Feng and Gray, 2017; Kang et al., 2019). In the initial stage of injection (Fig. 15a and c), the gel entered the fracture as a suspension with the fluid from the inlet. The contact time of the gel with oil was short, and their particle sizes remained small. The settling velocity of the particles was slow under the action of the fluid driving force, thereby the particles tended to disperse. With the inlet as the baseline, the particles migrated forward and expanded slowly to both sides (Wang et al., 2020a,b). The settling of the particles was limited at the inlet under the action of the fluid driving force. In the middle stage of particle migration, the gel could freely pass in the fracture, completely pass through the fracture under pressure, and migrate to the exit. At this stage, effective plugging could not be achieved, and the fluid at the central baseline flowed back to both sides due to friction. The back-flowing fluid encountered the extended fluid on both sides and slowly extended to both sides (Xu et al., 2018). During the entire process, the oil-absorbing gel migrated toward low concentration, and the particles became more dispersed and loose in the fluid. At this time, the collision between the particles was weakened, and the contact area was small; thus, the particles were not subjected to deformation and compression (Xu et al., 2019). In the final stage of particle migration, the fluid driving force on the central baseline weakened, leading to a reduced migration velocity of the particles and gradually increased viscosity coefficient of the fluid. As a result, the collision between the particles increased, and the particles aggregated from dispersion and deformed gradually under extrusion (Guo et al., 2015).

In a solid–liquid two-phase flow, the migration process of a single particle gel is determined by the fluid and the adjacent particles. This migration process can be divided into the suspension process under the action of the fluid and the mutual collision process between the gel (Civan, 2016). The dynamic change process of the gel in the microscopic perspective is shown in Fig. 16a–d. In the initial stage of entering the fracture, a diffused double layer was formed on the surface of the particles after they met oil. This formation of the double layer was due to a large number of lipophilic groups on the particle surface. The contact time between the gel and the oil was short; hence, the oil absorption capacity was low and the particle size was small. The contact area between the gel was small, and the particles could smoothly pass through the fracture area with the fluid. At this stage, the gel was mainly governed by the combined effect of their own gravity F_g, fluid driving force F_d, and wall friction F_f, as shown in Fig. 17. With the continuous contact between the particles and oil molecules, a concentration difference between the inside and outside of the polymer network was generated. Under van der Waals force, osmotic pressure difference, and capillary force, the oil molecules continuously entered the polymer network. As a result, the gel swelled continuously in the oil medium, and the particle size gradually increased. The relative concentration of the gel in the fluid was low, and the particles were hardly captured by the fracture wall and tended to disperse in the fluid under continuous injection pressure (Hu et al., 2018). As the oil molecules continuously entered the gel structure, both the volume and concentration of the gel kept increasing. At this time, the gel was subjected to the dragging force of the fluid and the contact force between the gel. The contact force can be further resolved into elastic and damping forces. One particle could simultaneously collide with multiple particles, resulting in the slowing down of the migration velocity of the particles under continuous collision.

4.2. Plugging mechanism

The size of conventional bridging material is smaller than the fracture width; thus, the material does not exert force inside the fracture during migration with the drilling fluid. Therefore, retaining the lost circulation material in fractures is difficult. According to the result of stress–strain test of the oil-absorbing gel, the maximum elongation of the gel reaches 1680%, and the maximum fracture stress is 159.3 kPa. Therefore, the oil-absorbing gel belongs to deformation materials, and their sizes can change from microns to the maximum width of the fracture because of their superior elasticity. Therefore, the gel can be squeezed into the fracture under pressure and can produce a large reaction force towards the inner wall of the fracture; thereby, the particles are easily retained in the lost circulation channels.

Under the action of combined forces inside the fracture, the oil-absorbing gel is likely to single-particle bridging, double-particle bridging, and multi-particle bridging. As shown in Fig. 18a, the oil-absorbing gel continuously absorbed oil and swelled in the oil, with their size exceeding the throat of the fracture channel. The gel kept migrating forward under fluid driving force and deformed due to their friction and extrusion with the fracture wall during the

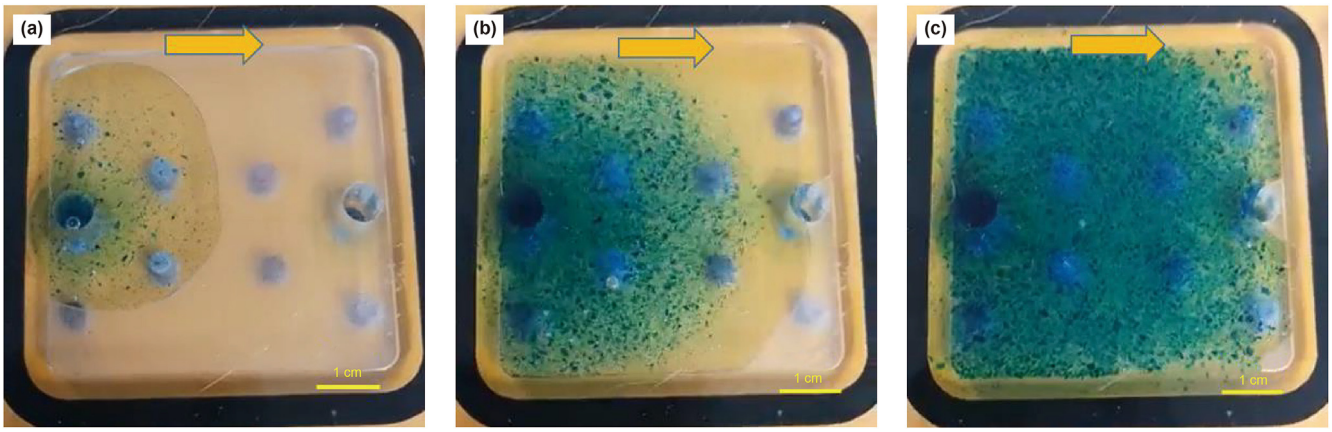

Fig. 15. Macroscopic migration process of oil-absorbing gel in fracture. (**a**) Flow state at early stage of gel migration in fracture; (**b**) flow state at middle stage of gel migration in fracture; (**c**) flow state at later stage of gel migration in fracture.

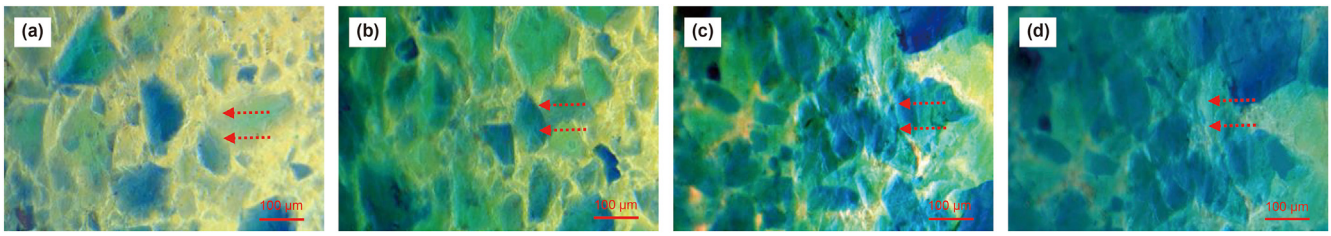

Fig. 16. Microscopic migration process of oil-absorbing gel in fracture. (**a**) Gel just enters fracture; (**b**) gel migrates in suspension in fracture; (**c**) gel collides and aggregate in fracture; (**d**) gel expands and deforms in fracture.

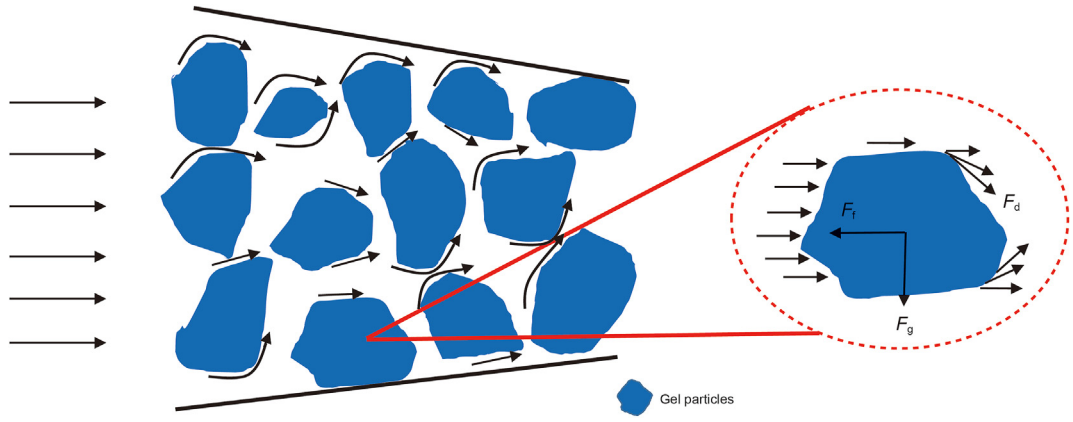

Fig. 17. Schematic diagram of force analysis of oil-absorbing gel in migration stage in fracture. F_d is the driving force of drilling fluid on oil-absorbing gel, F_g is the gravity of oil-absorbing gel, F_f is the friction among oil-absorbing gel and fracture wall.

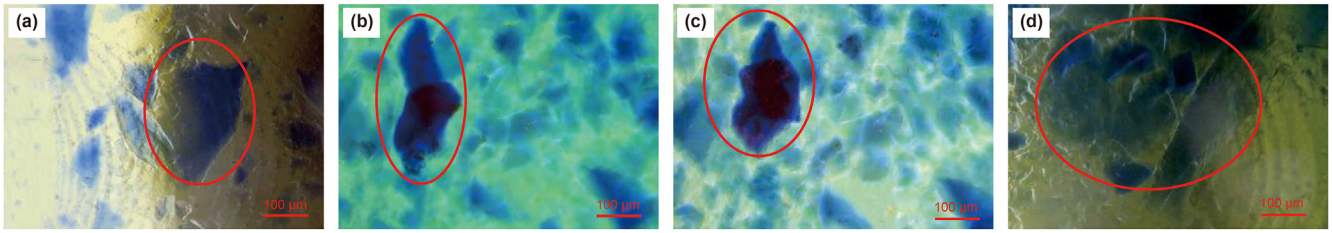

Fig. 18. Bridge plugging effect of oil-absorbing gel in fracture. (**a**) Plugging effect of single particle gel in fracture; (**b**) bridging effect of double particle gel in fracture; (**c**) plugging effect of double particle gel in fracture; (**d**) plugging effect of multi particle gel in fracture.

migration process. A single particle gel was stuck at the throat of the fracture and led to a single particle bridging, forming the basic skeleton plugging the loss channel and thereby reducing the original fracture channel space. Under the action of pressure difference, small size particles filled up the space progressively to form a dense plugging layer (Alsaba et al., 2017). As shown in Fig. 18c, two particles smaller than the width of the fracture migrated with the fluid to the throat. Furthermore, the particles extruded and deformed at the throat, forming a double-particle bridging. The gel was significantly affected by gravity when migrating in the fracture, and they were retained on the fracture wall (Xu et al., 2017). The probability of collision between particles increased for the subsequent gel entering the fracture; consequently, the migration resistance increased. The particles then extruded and deformed under the action of the fluid driving force, thus forming a double-particle bridging. As the gel gradually migrated to the deep part of the fracture, the fluid driving force on the particles gradually decreased (Fig. 18d). In addition, the fracture surface was uneven and rough, and the particles were easily trapped by the fracture after coming in contact with the fracture surface (She et al., 2020b). Along with the increase in the number of multiple particles (particle size < fracture width) migrating to the fracture throat with the fluid, the degree of particle collision continuously increased. At this time, the gel settled, accumulated, continuously absorbed the oil, and swelled, thus forming a multi-particle bridging where small-size particle gels continuously accumulated and filled to form a fracture plugging layer. In addition to the bridging effect of particles in fracture plugging, the progressive filling and accumulation of the particles in the fracture are also important (Xu et al., 2020). Fracture plugging is a bridging and progressive filling process. The particle gels are mainly divided into three levels: (1) bridging particles, whose particle sizes match the fracture width, (2) progressive filling particles, and (3) minimum filling particles, as shown in Fig. 19. The progressive filling process determines the final permeability and density of the plugging layer, which effectively enhances the bearing resistance of the plugging layer.

Under a certain particle size combination, the gel has a synergistic effect. These particles are extruded and closely combined with each other, forming a stable force chain network in the pores or microfractures to enhance the bearing pressure capacity of the

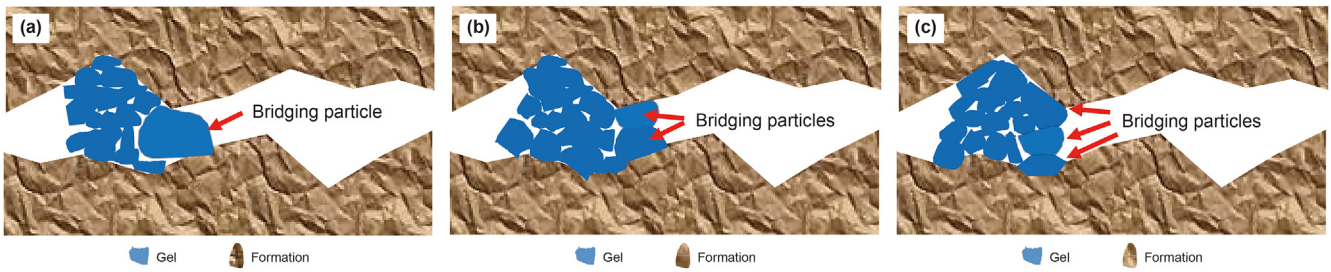

Fig. 19. Schematic diagram of bridge plugging effect of oil-absorbing gel in fracture. (**a**) Plugging effect of single particle gel in fracture; (**b**) plugging effect of double particle gel in fracture; (**c**) plugging effect of multi particle gel in fracture.

plugging layer (Yan et al., 2020). For fracture lost circulation, the key to the lost circulation control is a particle gel bridging in the fracture, which lays the foundation for the formation of a stable plugging layer. According to the experimental results and analysis of the actual circulation control process, the lost circulation material is present in three states in the fracture: "sealing throat," "sealing waist," and "sealing tail." To further study the corresponding processes, the accumulation and filling effects of the gel at the entrance, internal space (top and bottom of the fracture), and exit of the fracture were investigated, and the mechanism of the gel forming a plugging layer in the fracture was analyzed.

4.2.1. Plugging behavior of gel at fracture entrance

The dynamic filling process of the oil-absorbing gel at the entrance of the fracture model is shown in Fig. 20. In the initial stage, the gel continuously entered into the fracture under the driving force of drilling fluid and was suspended in the oil medium. From the microscopic point of view, the gel was dispersed, and the mutual contact force among the particles was small. With the continuous injection of the liquid, the large particle gel was extruded and deformed under pressure, forming a loose bridging layer at the entrance of the fracture; while the small particle gel was retained into the bridging layer (Fig. 20a and b). Under the action of an external load, the gel extruded with each other, resulting in different contact stresses. The contact force propagated along the particles to form a weak force chain network structure (Yan et al., 2021). Owing to the short oil absorption time, the expansion and deformation extrusion stress between the particles was small. With the continuous increase in the injection volume, the pressure at the entrance kept increasing, destabilizing the weak force chain network structure at the entrance. Therefore, under the action of the fluid driving force, the loose bridging layer was destroyed, the particle gel slipped to the exit, and the solid-phase particle aggregates gradually shifted to a discrete disordered state (Fig. 20c and d). The weak force chain network was gradually destroyed, and only the bridging particles remained in the fracture (Alshubbar et al., 2018). As the gels kept absorbing oil continuously, many particle gels aggregated again at the fracture entrance to form the bridging layer (Fig. 20e and f). As a result, the original lost circulation channel became narrow, small particles progressively filled and compacted the bridging layer to form a dense plugging layer, and a strong chain network structure was finally formed (Fig. 20g and h). Upon the gradual formation of the plugging layer, the internal particles were subjected to the driving force of drilling fluid (F_d), the extrusion force of fracture wall (F_w), and the extrusion force among the gel after expansion (F_e) generated by the continuous absorbing of the gel (Fig. 21) (She et al., 2020a).

4.2.2. Plugging behavior of gel at fracture top and bottom

The dynamic filling process of the oil-absorbing gel at the top and bottom of the fracture model is shown in Fig. 22a–d. In the initial stage, many discrete particle gels continuously migrated to the exit of the fracture under the driving force of drilling fluid (Fig. 22a). At this time, because the oil absorption time was short and a bridge plugging was not formed, the gel was in a disordered state and the contact stress among particles was small. Some of the particle gels settled under centrifugal force and gravity and aggregated on the upper and lower sides of the fracture model,

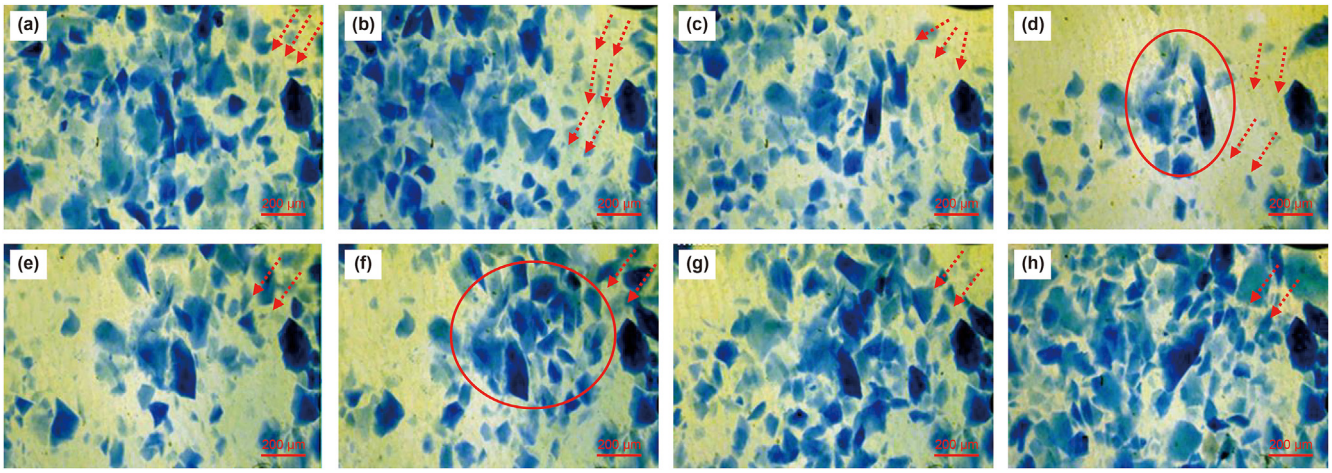

Fig. 20. Aggregation and filling process of oil-absorbing gel at different times at fracture entrance. (**a, b**) Large particle gel absorbs oil and expands to form a loose bridging layer; (**c, d**) the loose bridging layer is destroyed and the gel shows a discrete disordered state; (**e, f**) gel aggregates again at the fracture entrance to form the bridging layer; (**g, h**) gel forms a compacted and dense plugging layer.

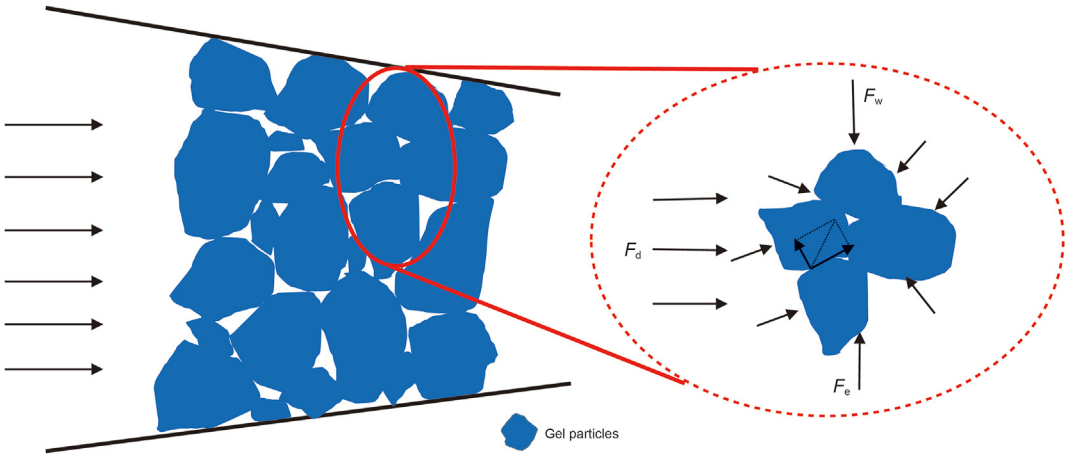

Fig. 21. Schematic diagram of force analysis of oil-absorbing gel after compaction and filling in fracture. F_d is the driving force of drilling fluid on gel, F_w is the extrusion force of fracture wall on gel, and F_e is the extrusion force among gel after expansion.

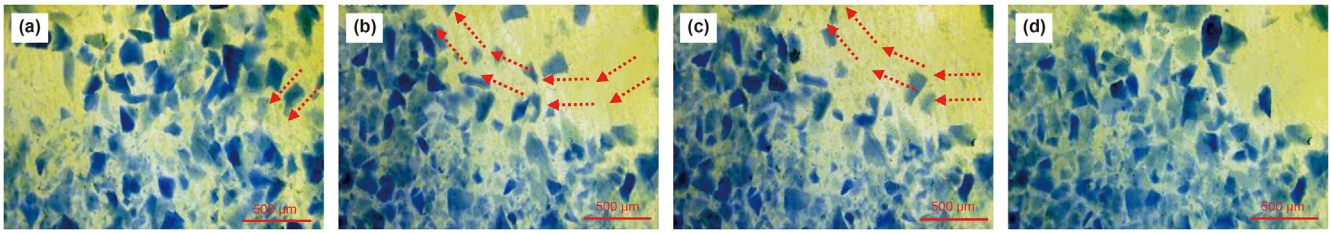

Fig. 22. Aggregation and filling process of oil-absorbing gel at different times at fracture top and bottom. (**a**) Low concentration gel at discrete state by the driving force of drilling fluid; (**b**) gel is deposited at fracture top and bottom; (**c**) gel aggregates at fracture top and bottom; (**d**) gel fills the fracture top and bottom and forms compacted gel plugging layer.

forming an arc-shaped deposition with the entrance of the fracture as the center (Fig. 22b). In addition, the gel continuously absorbed the oil and swelled, the interaction force among particles gradually increased, and the particles became gradually dense on both sides of the fracture (Fig. 22c). The gel on the inner side overcame the frictional force at the particle boundary and gradually migrated toward the fracture exit under the fluid-dragging force. With the continuous fluid injection, the bridging and filling of the particles proceeded gradually at the upper and lower sides of the fracture and continuously absorbed the oil and swelled, forming a plugging layer with a certain bearing pressure capacity (Fig. 22d) (Zhang et al., 2020). At this time, the particles were closely stacked and extruded, generating contact stress of different magnitudes. The shear resistance capacity of the gel enhanced significantly, and the flow resistance gradually increased. Differently from the phenomenon that most of rigid particles remained at the fracture entrance, the retention of the gel shifted gradually from fracture exit to fracture entrance, thereby gradually forming a dense plugging zone.

4.2.3. Plugging behavior of gel at fracture exit

The dynamic aggregation and filling process of the oil-absorbing gel at the exit of the fracture model is shown in Fig. 23. The gel entered the fracture with the fluid. The gel density in the fluid was low, and the friction among particles and the fracture wall was small; hence, the particle retention capacity was poor. Owing to the pressure difference between the entrance and exit of the fracture, the gel rapidly surged to the exit (Fig. 23a). As the particles continued absorbing, the reaction force among the particle larger than the fracture and the fracture wall was generated. Moreover, the fluid driving force was lower than the gravitational force of the particles and the wall friction, forming particle bridging and thereby reducing the space of the original lost circulation channel at the exit (Fig. 23b). Under the continuous effect of the fluid driving force, the gel gradually slid toward the bridging particles and continuously accumulated at the bridging particles, forming small linkages through extrusion under external load (Fig. 23c). Meanwhile, the bridging particles supported each other to form a stable aggregate (Nie et al., 2022). At this time, the flow resistance at the exit gradually increased, and the small particles continuously embedded in and filled the space between the bridging particles, thus gradually forming a dense large-scale accumulation (Fig. 23d). In additional to their progressive filling, the particles were densely packed and extruded to form a plugging layer (Fig. 23e and f) (Fang et al., 2020). Macroscopically, fine particles gradually filled the space and stacked closely to form an arc-shaped accumulation with the exit of the fracture as the center. Microscopically, the particles absorbed oil and swelled, producing different degrees of contact stress through an extrusion, and forming force chain structures of different strengths. The force chain structures then interlocked to form a force chain network and penetrated the plugging layer.

5. Conclusions

An oil-absorbing gel with favorite oil absorption capacity and plugging performance was prepared using rigid and flexible chain monomers simultaneously, and the microscopic plugging mechanism was investigated in detail.

(1) The oil absorption capacity of the gel was good. The oil absorption capacity of the gel reached 20.93 g/g at a high temperature of 140 °C. It increased with the extension of

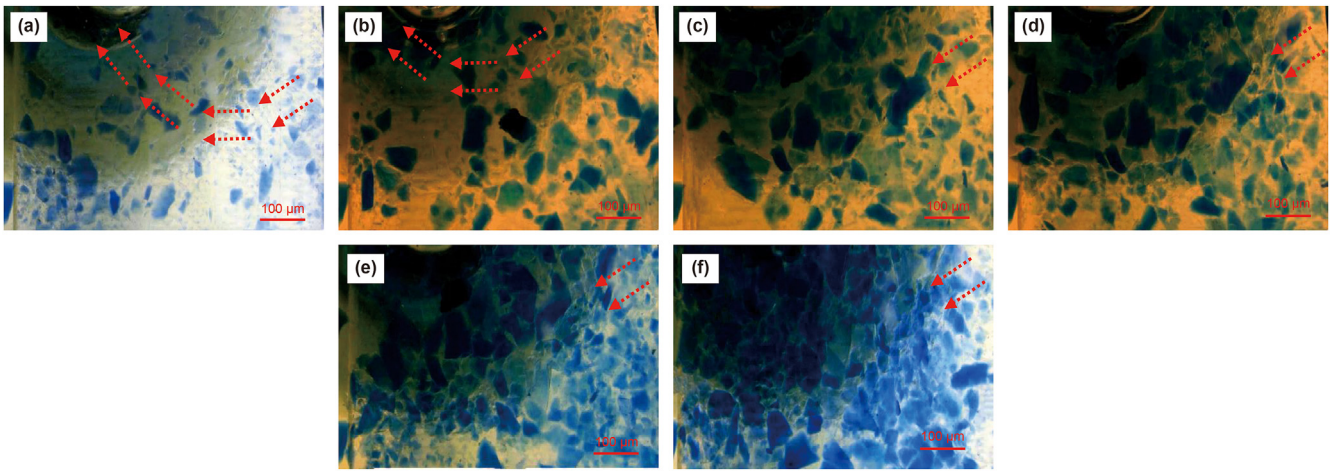

Fig. 23. Aggregation and filling process of oil-absorbing gel at different times at fracture exit. (**a**) Gel migrates by the driving force of drilling fluid; (**b**) gel bridges at fracture exit; (**c**) gel aggregates at fracture exit; (**d**) gel aggregates at fracture exit in a large scale; (**e**) gel fills the fracture exit; (**f**) gel plugging layer is formed and compacted at fracture exit.

time and the increase in temperature, and changed slight with the pressure.

(2) The plugging performance of the oil-absorbing gel was satisfactory. The optimal formula contains 2% gel with the size of 0.6 mm, 2% gel with the size of 0.3 mm, and 1% gel with the size of 0.2 mm, which can prevent the drilling fluid loss in porous media. In addition, the bearing pressure capacity of the gel reached 6.72 MPa for a fracture with exit width of 3 mm at 140 °C.

(3) The oil-absorbing gel can form a plugging zone in fractures through oil absorbing, elastic deformation, bridging-plugging, deposition-filling, and extrusion-accumulation. Increasing the accumulation and filling degree of the gel with different sizes effectively enhanced its plugging performance.

Declaration of competing interest

The authors declare that they have no known competing financial interests or personal relationships that could have appeared to influence the work reported in this paper.

Acknowledgments

This research is financially supported by the National Natural Science Foundation of China (Grant 52074327, 51991361), the Natural Science Foundation of Shandong Province, China (ZR2020QE107).

References

Abrams, A., 1997. Mud design to minimize rock impairment due to particle invasion. J. Petrol. Technol. 29 (5), 586–592. https://doi.org/10.2118/5713-PA.

Alsaba, M., Al Dushaishi, M.F., Nygaard, R., et al., 2017. Updated criterion to select particle size distribution of lost circulation materials for an effective fracture sealing. J. Petrol. Sci. Eng. 149, 641–648. https://doi.org/10.1016/j.petrol.2016.10.027.

Alshubbar, G., Nygaard, R., Jeennakorn, M., 2018. The effect of wellbore circulation on building an LCM bridge at the fracture aperture. J. Petrol. Sci. Eng. 165, 550–556. https://doi.org/10.1016/j.petrol.2018.02.034.

Alves, M.D., Aracri, F.M., Cren, É.C., et al., 2017. Isotherm, kinetic, mechanism and thermodynamic studies of adsorption of a microbial lipase on a mesoporous and hydrophobic resin. Chem. Eng. J. 311, 1–12. https://doi.org/10.1016/j.cej.2016.11.069.

Aston, M.S., Alberty, M.W., McLean, M.R., et al., 2004. Drilling fluids for wellbore strengthening. In: IADC/SPE Drilling Conference. https://doi.org/10.2118/87130-MS.

Bai, Y., Shang, X., Wang, Z., et al., 2018. Experimental study of low molecular weight polymer/nanoparticle dispersed gel for water plugging in fractures. Colloids Surf. A Physicochem. Eng. Asp. 551, 95–107. https://doi.org/10.1016/j.colsurfa.2018.04.067.

Bai, Y., Zhang, Q., Sun, J., et al., 2021a. Self-healing hydrogels and their action mechanism in oil–gas drilling and development engineering: a systematic review and prospect. J. Nat. Gas Sci. Eng. 96, 104250. https://doi.org/10.1016/j.jngse.2021.104250.

Bai, Y., Zhang, Q., Sun, J., et al., 2021b. Disproportionate filtration behaviors of polymer/chromium gel used for fracture plugging. J. Mol. Liq. 343, 117567. https://doi.org/10.1016/j.molliq.2021.117567.

Bu, X., Lu, Y., Chen, S., et al., 2019. Fabrication of porous carbon nitride foams/acrylic resin composites for efficient oil and organic solvents capture. Chem. Eng. J. 355, 299–308. https://doi.org/10.1016/j.cej.2018.08.088.

Calçada, L.A., Duque Neto, O.A., Magalhães, S.C., et al., 2015. Evaluation of suspension flow and particulate materials for control of fluid losses in drilling operation. J. Petrol. Sci. Eng. 131, 1–10. https://doi.org/10.1016/j.petrol.2015.04.007.

Chen, C., Cai, L., Zhang, L., et al., 2020. Transesterification of rice bran oil to biodiesel using mesoporous NaBeta zeolite-supported molybdenum catalyst: experimental and kinetic studies. Chem. Eng. J. 382 122839. https://doi.org/10.1016/j.cej.2019.122839.

Chen, Y., Wu, R., Zhou, J., et al., 2021. A novel hyper-cross-linked polymer for high-efficient fluid-loss control in oil-based drilling fluids. Colloids Surf. A Physicochem. Eng. Asp. 626 127004. https://doi.org/10.1016/j.colsurfa.2021.127004.

Civan, F., 2016. Modified formulations of particle deposition and removal kinetics in saturated porous media. Transport Porous Media 111 (2), 381–410. https://doi.org/10.1007/s11242-015-0600-z.

Cohen, N., McMeeking, R.M., 2019. On the swelling induced microstructural evolution of polymer networks in gels. J. Mech. Phys. Solid. 125, 666–680. https://doi.org/10.1016/j.jmps.2019.01.018.

Cui, K.-X., Jiang, G.-C., Yang, L.-L., et al., 2021. Preparation and properties of magnesium oxysulfate cement and its application as lost circulation materials. Petrol. Sci. 18 (5), 1492–1506. https://doi.org/10.1016/j.petsci.2021.08.002.

Deng, J., Yang, B., Chen, C., et al., 2015. Renewable eugenol-based polymeric oil-absorbent microspheres: preparation and oil absorption ability. ACS Sustain. Chem. Eng. 3 (4), 599–605. https://doi.org/10.1021/sc500724e.

Deng, Y., Han, D., Deng, Y.-Y., et al., 2020. Facile one-step preparation of robust hydrophobic cotton fabrics by covalent bonding polyhedral oligomeric silsesquioxane for ultrafast oil/water separation. Chem. Eng. J. 379 122391. https://doi.org/10.1016/j.cej.2019.122391.

Du, H., Li, S., Qu, H., et al., 2018. Stable cycling of lithium-sulfur battery enabled by a reliable gel polymer electrolyte rich in ester groups. J. Membr. Sci. 550, 399–406. https://doi.org/10.1016/j.memsci.2018.01.017.

Ezeakacha, C.P., Salehi, S., Kiran, R., 2018. Lost circulation and filter cake evolution: impact of dynamic wellbore conditions and wellbore strengthening implications. J. Petrol. Sci. Eng. 171, 1326–1337. https://doi.org/10.1016/j.petrol.2018.08.063.

Fang, Y., Guo, L., Hou, M., 2020. Arching effect analysis of granular media based on force chain visualization. Powder Technol. 363, 621–628. https://doi.org/10.1016/j.powtec.2020.01.038.

Feng, Y., Gray, K.E., 2017. Review of fundamental studies on lost circulation and wellbore strengthening. J. Petrol. Sci. Eng. 152, 511–522. https://doi.org/10.1016/j.petrol.2017.01.052.

Feng, Y., Li, X., Gray, K.E., 2018. An easy-to-implement numerical method for quantifying time-dependent mudcake effects on near-wellbore stresses. J. Petrol. Sci. Eng. 164, 501–514. https://doi.org/10.1016/j.petrol.2018.01.051.

Gautam, S., Guria, D., Rajak, V.K., 2022. A state of the art review on the performance

of high-pressure and high-temperature drilling fluids: towards understanding the structure-property relationship of drilling fluid additives. J. Petrol. Sci. Eng. 213, 110318. https://doi.org/10.1016/j.petrol.2022.110318.
Guo, Z., Chen, X., Xu, Y., et al., 2015. Effect of granular shape on angle of internal friction of binary granular system. Fuel 150, 298–304. https://doi.org/10.1016/j.fuel.2015.02.047.
Ho, Y.S., McKay, G., 1999. The sorption of lead(II) ions on peat. Water Res. 33 (2), 578–584. https://doi.org/10.1016/S0043-1354(98)00207-3.
Hu, Y., Yang, J., Wang, J., et al., 2018. Investigation of hydrodynamic and heat transfer performances in grille-sphere composite pebble beds with DEM-CFD-Taguchi method. Energy 155, 909–920. https://doi.org/10.1016/j.energy.2018.05.018.
Jiang, G., Sun, J., He, Y., et al., 2021. Novel waterbased drilling and completion fluid technology to improve wellbore quality during drilling and protect unconventional reservoirs. Engineering. https://doi.org/10.1016/j.eng.2021.11.014.
Jiang, G., Shi, H., He, Y., 2022. The biodiesel-based flat-rheology drilling fluid system. Petrol. Explor. Dev. 49 (1), 173–182. https://doi.org/10.11698/PED.2022.01.16.
Kang, Y., Xu, C., Tang, L., et al., 2014. Constructing a tough shield around the wellbore: theory and method for lost-circulation control. Petrol. Explor. Dev. 41 (4), 520–527. https://doi.org/10.1016/S1876-3804(14)60061-6.
Kang, Y., Tan, Q., You, L., et al., 2019. Experimental investigation on size degradation of bridging material in drilling fluids. Powder Technol. 342, 54–66. https://doi.org/10.1016/j.powtec.2018.09.086.
Kundu, P., Mishra, I.M., 2013. Removal of emulsified oil from oily wastewater (oil-in-water emulsion) using packed bed of polymeric resin beads. Separ. Purif. Technol. 118, 519–529. https://doi.org/10.1016/j.seppur.2013.07.041.
Lavrov, A., 2016. Lost Circulation: Mechanisms and Solutions. Gulf Professional Publishing, London. https://doi.org/10.1016/C2015-0-00926-1.
Lei, X., Ye, D., Chen, J., et al., 2019. Customizable multidimensional self-wrinkling structure constructed via modulus gradient in chitosan hydrogels. Chem. Mater. 31, 10032–10039. https://doi.org/10.1021/acs.chemmater.9b02812.
Lei, S., Sun, J., Bai, Y., et al., 2022. Formation mechanisms of fracture plugging zone and optimization of plugging particles. Petrol. Explor. Dev. 49 (3), 597–604. https://doi.org/10.11698/PED.20210677.
Li, Y., 2013. Effects of particle shape and size distribution on the shear strength behavior of composite soils. Bull. Eng. Geol. Environ. 72 (3), 371–381. https://doi.org/10.1007/s10064-013-0482-7.
Li, W., Zhao, X., Ji, Y., et al., 2016. Investigation of biodiesel-based drilling fluid, part 1: biodiesel evaluation, invert-emulsion properties, and development of a novel emulsifier package. SPE J. 21 (5), 1755–1766. https://doi.org/10.2118/180926-PA.
Li, W., Jiang, G., Ni, X., et al., 2020. Styrene butadiene resin/nano-SiO_2 composite as a water-and-oil-dispersible plugging agent for oil-based drilling fluid. Colloids Surf. A Physicochem. Eng. Asp. 606 125245. https://doi.org/10.1016/j.colsurfa.2020.125245.
Li, R., Li, G., Feng, Y., et al., 2022. Innovative experimental method for particle bridging behaviors in natural fractures. J. Nat. Gas Sci. Eng. 97, 104379. https://doi.org/10.1016/j.jngse.2021.104379.
Nie, Z., Qi, Q., Wang, X., et al., 2022. DEM investigation of strain behaviour and force chain evolution of gravel–sand mixtures subjected to cyclic loading. Particuology 68, 13–28. https://doi.org/10.1016/j.partic.2021.10.006.
Pang, H., Meng, H., Wang, H., et al., 2022. Lost circulation prediction based on machine learning. J. Petrol. Sci. Eng. 208 109364. https://doi.org/10.1016/j.petrol.2021.109364.
Qiu, J., Bai, Y., Sun, J., et al., 2022. Experimental study on an oil-based polymer gel for lost circulation control in high-temperature fractured formation. J. Appl. Polym. Sci. 139 (10), 51763. https://doi.org/10.1002/app.51763.
Rong, J., Qiu, F., Zhang, T., et al., 2017. A facile strategy toward 3D hydrophobic composite resin network decorated with biological ellipsoidal structure rapeseed flower carbon for enhanced oils and organic solvents selective absorption. Chem. Eng. J. 322, 397–407. https://doi.org/10.1016/j.cej.2017.04.049.
Sauerwein, M., Steeb, H., 2020. Modeling of dynamic hydrogel swelling within the pore space of a porous medium. Int. J. Eng. Sci. 155, 103353. https://doi.org/10.1016/j.ijengsci.2020.103353.
She, J., Zhang, H., Han, K., et al., 2020a. Experimental investigation of mechanisms influencing friction coefficient between lost circulation materials and shale rocks. Powder Technol. 364, 13–26. https://doi.org/10.1016/j.powtec.2020.01.047.
She, J., Zhang, H., Kang, Y., et al., 2020b. Cusp catastrophe model for plugging pressure prediction of lost circulation control in fractured reservoirs. J. Petrol. Sci. Eng. 186, 106705. https://doi.org/10.1016/j.petrol.2019.106705.
Sokker, H.H., El-Sawy, N.M., Hassan, M.A., et al., 2011. Adsorption of crude oil from aqueous solution by hydrogel of chitosan based polyacrylamide prepared by radiation induced graft polymerization. J. Hazard Mater. 190 (1), 359–365. https://doi.org/10.1016/j.jhazmat.2011.03.055.
Song, Z., Bai, B., Zhang, H., 2018. Preformed particle gel propagation and dehydration through semi-transparent fractures and their effect on water flow. J. Petrol. Sci. Eng. 167, 549–558. https://doi.org/10.1016/j.petrol.2018.04.044.
Sun, J., Bai, Y., Cheng, R., et al., 2021. Research progress and prospect of plugging technologies for fractured formation with severe lost circulation. Petrol. Explor. Dev. 48 (3), 732–743. https://doi.org/10.1016/S1876-3804(21)60059-9.
Tariq, Z., Mahmoud, M., Alahmar, M., et al., 2022. Lost circulation mitigation using modified enzyme induced calcite precipitation technique. J. Petrol. Sci. Eng. 210 110043. https://doi.org/10.1016/j.petrol.2021.110043.
van Oort, E., Incedalip, O., Vajargah, A., 2018. Thermal wellbore strengthening through managed temperature drilling – Part I: thermal model and simulation. J. Nat. Gas Sci. Eng. 58, 275–284. https://doi.org/10.1016/j.jngse.2018.06.046.
Wang, H., Chen, M., Wei, S., et al., 2020a. The influence of barrier coastal sedimentary system lost circulation in sandstone. J. Petrol. Sci. Eng. 185 106654. https://doi.org/10.1016/j.petrol.2019.106654.
Wang, M.-B., Guo, Y.-L., Chen, W.-Q., 2020b. Effect of solid particles on the lost circulation of drilling fluid: a numerical simulation. Powder Technol. 363, 408–418. https://doi.org/10.1016/j.powtec.2019.12.029.
Xu, C., Kang, Y., You, L., et al., 2017. Lost-circulation control for formation-damage prevention in naturally fractured reservoir: mathematical model and experimental study. SPE J. 22 (5), 1654–1670. https://doi.org/10.2118/182266-PA.
Xu, C., You, Z., Kang, Y., et al., 2018. Stochastic modelling of particulate suspension transport for formation damage prediction in fractured tight reservoir. Fuel 221, 476–490. https://doi.org/10.1016/j.fuel.2018.02.056.
Xu, C., Yan, X., Kang, Y., et al., 2019. Friction coefficient: a significant parameter for lost circulation control and material selection in naturally fractured reservoir. Energy 174, 1012–1025. https://doi.org/10.1016/j.energy.2019.03.017.
Xu, C., Yan, X., Kang, Y., et al., 2020. Structural failure mechanism and strengthening method of fracture plugging zone for lost circulation control in deep naturally fractured reservoirs. Petrol. Explor. Dev. 47 (2), 430–440. https://doi.org/10.1016/S1876-3804(20)60060-X.
Xu, C., Zhang, H., Zhu, M., et al., 2021a. Experimental study on the controlling factors of frictional coefficient for lost circulation control and formation damage prevention in deep fractured tight reservoir. Petroleum. https://doi.org/10.1016/j.petlm.2021.10.015.
Xu, C., Zhang, J., Kang, Y., et al., 2021b. Structural formation and evolution mechanisms of fracture plugging zone. Petrol. Explor. Dev. 48 (1), 232–242. https://doi.org/10.1016/S1876-3804(21)60019-8.
Yan, X., Kang, Y., Xu, C., et al., 2020. Fracture plugging zone for lost circulation control in fractured reservoirs: multiscale structure and structure characterization methods. Powder Technol. 370, 159–175. https://doi.org/10.1016/j.powtec.2020.05.026.
Yan, X., Kang, Y., Xu, C., et al., 2021. Impact of friction coefficient on the mesoscale structure evolution under shearing of granular plugging zone. Powder Technol. 394 133–148. https://doi.org/10.1016/j.powtec.2021.08.005.
Yang, P., Hu, X., Tu, Y., et al., 2021. The synthesis of a DMpillar[5]arene-based porous polymer with ultrafast adsorption rate and high adsorption capacity for organic micropollutants from water. Chem. Eng. J., 132418 https://doi.org/10.1016/j.cej.2021.132418.
Yang, S., Osipov, Y., Xu, C., et al., 2022. Analytical solution for large-deposit nonlinear reactive flows in porous media. Chem. Eng. J. 430 132812. https://doi.org/10.1016/j.cej.2021.132812.
Yao, C., Lei, G., Cathles, L.M., et al., 2014. Pore-scale investigation of micron-size polyacrylamide elastic microspheres (MPEMs) transport and retention in saturated porous media. Environ. Sci. Technol. 48 (9), 5329–5335. https://doi.org/10.1021/es500077s.
Yao, C., Liu, B., Li, L., et al., 2020. Transport and retention behaviors of deformable polyacrylamide microspheres in convergent–divergent microchannels. Environ. Sci. Technol. 54 (17), 10876–10884. https://doi.org/10.1021/acs.est.0c02243.
Yu, C., Jiang, Je, Liu, Y., et al., 2021. Facile fabrication of compressible, magnetic and superhydrophobic poly(DVB-MMA) sponge for high-efficiency oil–water separation. J. Mater. Sci. 56 (4), 3111–3126. https://doi.org/10.1007/s10853-020-05471-z.
Zhang, T., Kong, L., Dai, Y., et al., 2017. Enhanced oils and organic solvents absorption by polyurethane foams composites modified with MnO_2 nanowires. Chem. Eng. J. 309, 7–14. https://doi.org/10.1016/j.cej.2016.08.085.
Zhang, T., Li, Z., Lü, Y., et al., 2019. Recent progress and future prospects of oil-absorbing materials. Chin. J. Chem. Eng. 27, 1282–1295. https://doi.org/10.1016/j.cjche.2018.09.001.
Zhang, L., Zhou, F., Feng, W., et al., 2020. Experimental study on plugging behavior of degradable fibers and particulates within acid-etched fracture. J. Petrol. Sci. Eng. 185, 106455. https://doi.org/10.1016/j.petrol.2019.106455.
Zhong, H., Shen, G., Yang, P., et al., 2018. Mitigation of lost circulation in oil-based drilling fluids using oil absorbent polymers. Materials 11, 2020. https://doi.org/10.3390/ma11102020.